THESIS FOR THE DEGREE OF DOCTOR OF PHILOSOPHY

Weldability of Cast Superalloys

Effect of homogenization heat treatments on hot cracking susceptibility of cast Alloy 718, ATI® 718Plus®, and Haynes® 282®

Sukhdeep Singh

CHALMERS

Department of Industrial and Materials Science
CHALMERS UNIVERSITY OF TECHNOLOGY
Gothenburg, Sweden

Weldability of Cast Superalloys

Effect of homogenization heat treatments on hot cracking susceptibility of cast Alloy 718, ATI® 718Plus®, and Haynes® 282®

Sukhdeep Singh

ISBN: 978-91-7905-366-6
Doktorsavhandlingar vid Chalmers tekniska högskola, Ny series nr 4833
ISSN 0346-718X

Department of Industrial and Materials Science
Chalmers University of Technology
SE-412 96 Gothenburg
Sweden
Telephone + 46 (0)31-772 1000

Printed by Chalmers digitaltryck
Gothenburg, Sweden 2020

With the Blessings of Sri Guru Gobind Singh Ji

ਜਿਉ ਬੈਸੰਤਰਿ ਧਾਤੁ ਸੁਧੁ ਹੋਏ ਤਿਉ ਹਰਿ ਕਾ ਭਉ ਦੁਰਮਤਿ ਮੈਲੁ ਗਵਾਇ ॥
ਨਾਨਕ ਤੇ ਜਨ ਸੋਹਣੇ ਜਿ ਰਤੇ ਹਰਿ ਰੰਗੁ ਲਾਇ ॥

Just as the fire removes the impurities from the metal, so does the love of "*All Pervasive*" in removing the filth of the mind.
O Nanak! Those beings are beautiful, who are imbued with the love of "*All Pervasive*".

SGGS, Ang 1380

Weldability of Cast Superalloys

Effect of homogenization heat treatments on hot cracking susceptibility of cast Alloy 718, ATI® 718Plus® and Haynes® 282®

Sukhdeep Singh
Department of Industrial and Materials Science
Chalmers University of Technology

Abstract

Precipitation hardened Ni- and Ni–Fe-based superalloys are used in high-temperature sections of aero engines owing to their superior mechanical properties compared to those of the other alloys. However, their better mechanical performance is accompanied by its own challenges during the manufacturing process. For the fabrication of hot structural components, instead of the traditional single piece castings, welding is widely employed by joining wrought parts in sections, where high strength is required, and cast parts, where complex geometrical shapes are needed. This can be challenging, as superalloys are known for their lack of amenability to welding. A weld-cracking phenomenon known as "hot cracking" is of concern during their welding. Especially, the cast materials are known to be more prone to cracking owing to the higher extent of segregating phases that remain from the casting process.

The present study investigates the weldability of Alloy 718 and two recently developed Ni-based superalloys ATI® 718Plus® and Haynes® 282® with respect to heat affected zone liquation (HAZ) cracking susceptibility. Pre-weld homogenization treatments were performed at 1120 °C and 1190 °C to study the effect of different microstructures on cracking extent. The testing approach consisted of using Varestraint weldability test to assess the HAZ liquation cracking susceptibility and Gleeble thermomechanical simulator for evaluation of hot ductility behaviour. The results revealed that a lower heat treatment temperature at 1120 °C for 4 h was beneficial in minimizing the influence of liquation, and that the grain growth also contributed to lowering the cracking susceptibility in the HAZ. JMatPro simulations and microstructural evaluation on elements such as Nb as solute and precipitate former in Alloy 718 and ATI® 718Plus®, and Mo in Haynes® 282® were found to be important in the liquation mechanism. Secondary ion mass spectroscopy (SIMS) analysis revealed B, which is a strong melting point depressant, to segregate along the grain boundaries in all the three alloys. In addition, in this thesis, different liquation mechanisms were discussed and an explanation for the overall HAZ liquation cracking mechanism for cast superalloys was proposed.

Keywords: Nickel-based superalloys, Homogenization, Hot isostatic pressing, Welding, Varestraint, Gleeble, Hot cracking, Hot ductility, Niobium, Boron, Segregation

Preface

This doctoral thesis is based on a project work carried out in the Department of Industrial and Materials Science at Chalmers University of Technology, and at the Division of Welding Technology at University West between November 2015 and October 2020. This project was carried out under the supervision of Assoc. Professor Joel Andersson, and was financially supported by the Consortium of Materials and Technology for Thermal Energy Processes (KME) through a funding form the Swedish Energy Agency and GKN Aerospace Sweden AB. The support from SpaceLAB through the European Regional Development Fund is also gratefully acknowledged.

The thesis consists of an introductory part, followed by the appended papers listed below.

List of appended papers

Paper I: Hot cracking in cast Alloy 718
Sukhdeep Singh and Joel Andersson
Science and Technology of Welding and Joining, 2018, Volume 23, 568–574

Paper II: Influence of hot isostatic pressing on hot ductility of cast Alloy 718: Effect of niobium and minor elements on liquation mechanisms

Sukhdeep Singh, Fabian Hanning, and Joel Andersson
Metallurgical and Materials Transactions A, DOI: 10.1007/s11661-020-06004-8

Paper III: Varestraint weldability testing of cast ATI® 718 Plus™ – A comparison to cast Alloy 718
Sukhdeep Singh and Joel Andersson
Welding in the World, 2019, Volume 63, 389–399

Paper IV: Influence of homogenization treatment on hot ductility of Cast ATI® 718Plus®: Effect of niobium and minor elements on liquation characteristics

Sukhdeep Singh, Fabian Hanning, and Joel Andersson
Materials Science and Engineering: A, 2021, Volume 799, 140151

Paper V: Heat-affected zone liquation cracking in welded cast Haynes® 282®
Sukhdeep Singh and Joel Andersson
Metals 2020, Volume 10, Issue 1, 29

Contributions to the appended papers

Paper I: Assoc. Professor Joel Andersson planned the study. The author of this thesis planned and executed the microstructural investigations, analyzed the results, and prepared the manuscript with inputs provided by the co-author.

Paper II: Assoc. Professor Joel Andersson and this author planned the study. Dr. Fabian Hanning helped with the setup and training for Gleeble testing. The author planned and executed the hot ductility tests, as well as the microstructural investigations. Dr. Per Malmberg of the Department of Chemistry at Chalmers University of Technology performed the SIMS work. The author analyzed the results and prepared the manuscript with inputs from the co-authors.

Paper III: Assoc. Professor Joel Andersson planned the study. The author planned and executed part of the Varestraint testing with the help of Mr Kjell Hurtig, conducted the microstructural investigations, analyzed the results, and prepared the manuscript with inputs from the co-author.

Paper IV: Assoc. Professor Joel Andersson and the author planned the study. Dr. Fabian Hanning provided support for Gleeble testing. The author planned and executed the hot ductility tests, as well as the microstructural investigations. Dr. Per Malmberg of the Department of Chemistry at Chalmers University of Technology performed the SIMS work. The author analyzed the results and prepared the manuscript with inputs from the co-authors.

Paper V: Assoc. Professor Joel Andersson and the author planned the study. The author planned and executed the microstructural investigations. Dr. Aurelién Thomen from Gothenburg University performed the nanoSIMS work. The author analyzed the results and prepared the manuscript with inputs from the co-author.

Papers not appended to the thesis

Paper 1: Review of hot cracking phenomena in austenitic stainless steels
Sukhdeep Singh and Joel Andersson

7th International Swedish Production Symposium, SPS16, Lund, Sweden, October 25–27, 2016.

Swedish Production Academy, 2016, 1–7

Paper 2: Investigation on effect of welding parameters on solidification cracking of austenitic stainless steel 314
Sukhdeep Singh and Joel Andersson

Procedia Manufacturing, 2018, Volume 25, 351–357

Paper 3: Varestraint weldability testing of ATI® 718Plus® - Influence of eta phase
Sukhdeep Singh, William Fransson, Joel Andersson, Anssi Brederholm, and Hannu Hänninen

Proceedings of the 9th International Symposium on Superalloy 718 & Derivatives: Energy, Aerospace, and Industrial Applications, 2018, 917–928

Paper 4: A numerical model for simulating the effect of strain rate on eutectic band thickness
Joar Draxler, Paul Åkerström, Jonas Edberg, Lars-Erik Lindgren, Sukhdeep Singh, Tahira Raza and Joel Andersson
Welding in the World, 2020, Volume 64, 1635–1658

Table of Contents

1. Introduction

Ni- and Ni–Fe- based superalloys are the materials of choice in hot structural components of aero engines because of their high-temperature mechanical strength, and corrosion and oxidation resistance. The Ni–Fe-based Alloy 718, first developed in the 1960s [1], is still the most widely used superalloy at present. It has quickly emerged as the work-horse alloy in aerospace applications owing to its inherent resistance towards a solid-state cracking phenomenon known as "strain age cracking". Furthermore, it is also available in the cast form, made possible, by the development of vacuum melting technology [2]. However, its limitation has been a relatively low operating temperature of about 650 °C. To meet the demands of the aerospace industry for improved efficiency, two new Ni-based superalloys were introduced in the last decade, namely ATI® 718Plus® (ATI 718Plus) and Haynes® 282® (Haynes 282). Unlike Alloy 718, whose main strengthening precipitate is gamma double prime (γ′′), ATI 718Plus was developed with the more stable gamma prime (γ′) as its main strengthening precipitate, through careful alloy engineering, while maintaining the same fabricability as Alloy 718. The resulting alloy could operate at approximately 705 °C [3]. Similarly, optimum properties for cast Haynes 282 were achieved by designing it with a low fraction of γ′ so that it could operate at a maximum temperature of 800 °C, [4]. The initial research and development considered the wrought versions of ATI 718Plus and Haynes 282. The cast versions of ATI 718Plus and Haynes 282 are now under development for applications in large structural components [5].

Welding is an important process in a manufacturing chain. The recent trend in the aerospace industry is to join small castings or sheets together, for complex geometries and high strength sections, respectively, instead of using a large single piece casting. This helps in weight reduction, as well as reducing the manufacturing costs [6]. The wide range of alloying elements, which make up the chemical composition of an alloy, can often lead to formation of detrimental phases during welding, which in turn can lead to the cracking of the components. This phenomenon is known as "hot cracking", which occurs during the on-cooling thermal weld cycle owing to the inability of the grain boundaries to sustain the load because of the solidification shrinkage. In cast Alloy 718, the low-melting Laves phase is a major concern, as it aids in the formation a heat-affected zone (HAZ) cracking by liquation mechanism [7, 8]. Little is known regarding the behavior of the relatively new cast versions of ATI 718Plus and Haynes 282. Therefore, a thorough understanding of their metallurgy is crucial as cracking can lead to further complications in the workshop, requiring additional intervention through welding repairs and heat treatments.

Cast components often undergo homogenization heat treatments prior to welding. When it comes to cast components for structural applications, they typically undergo hot isostatic pressing (HIP) heat treatment to reduce the porosity and segregation, which are known to be not only detrimental for the mechanical properties, but also to the weldability. The HIP treatment approaches for cast Alloy 718 involve a partial

homogenization [9, 10] or total homogenization of the Laves phase [11]. However, in the case of cast ATI 718Plus and Haynes 282, there are no established standard homogenization treatments. Thus, very limited data and knowledge are available regarding the weldability and the mechanisms governing the HAZ liquation cracking of these new alloys.

1.1. Aim

The aim of this research is to obtain a fundamental knowledge on the HAZ liquation cracking, which is often encountered during the welding of Ni-based superalloys. The alloys investigated in this research are the cast superalloys — Alloy 718, ATI 718Plus, and Haynes 282, which are used for manufacturing hot structural components in aero engines. These components are subjected to homogenization heat treatment prior to welding. The HIP is often employed for cast structural components to eliminate any existing porosity, as well as reduce micro-segregation. The latter is known to influence the HAZ liquation cracking susceptibility. The HIP treatment of Alloy 718 involves dissolving the Laves phase at 1120 and 1190 °C. However, there are no standard homogenization approaches available for the recently developed cast versions of ATI 718Plus and Haynes 282. Therefore, the aim of this study is to investigate the effect of homogenization heat treatments on the weldability of the three cast superalloys Alloy 718, ATI 718Plus, and Haynes 282. Specifically, the following research objectives were formulated:

RQ 1: How do the microstructural changes that take place after the homogenization heat treatments, affect the HAZ liquation cracking susceptibility of cast superalloys – Alloy 718, ATI 718Plus, and Haynes 282?

RQ 2: What are the mechanisms in HAZ liquation cracking during the welding of these cast superalloys?

2. Cast superalloys

The chemical composition of superalloys consists of approximately 12–15 different elements, which render the microstructure very complex. These elements typically include Ni, Fe, Cr, Mo, Nb, Ti, Al, Co, Cu, W, C, Si, S, B, and P. Each of these elements has a specific role; elements, such as Fe, Co, Cr, and Mo confer solid solution strengthening in the γ matrix; Ni, Al and Ti are known to form the γ′ phase; while Ni and Nb form the γ′′ phase. Different types of carbides can form primary MC (Nb, Ti) as well as secondary carbides, which include $M_{23}C_6$ (Cr, Mo) and M_6C (Mo, W). The coarse primary carbides are generally considered detrimental for the mechanical properties; however, the secondary carbides, when uniformly dispersed along the grain boundaries as discrete precipitates, can inhibit grain boundary sliding and consequently, improve the strength. Apart from the strengthening phases and carbides, some Ni–Fe-based superalloys can contain topologically close-packed (TCP) phases, such as σ, μ and Laves. The TCP phases are generally considered detrimental, when present along the grain boundaries in a plate-like morphology, and can act as a source for crack initiation. Precipitation of other phases, such as η and δ, along the grain boundaries, are known to be very effective for grain size control [12]. Table 1 summarizes the types of precipitates and their chemistry, as observed in Ni- and Ni–Fe-based superalloys.

Table 1. Commonly found precipitates in Ni- and Ni–Fe-based superalloys [12], [13].

Phase	Crystal structure	Ni	Fe	Cr	Mo	Al	Ti	W	Co	Ta	Nb	Cl	Nb	B	Si	S
Matrix		×	×	×	×	×		×	×	×						
γ′	fcc	×				×	×									
γ′′′	bct	×									×	×				
MC	cubic			×	×		×	×		×	×					
$M_{23}C_6$	fcc		×	×	×			×	×							
M_6C	fcc	×			×			×	×							
δ	orthor.			×							×		×			
σ	tetrag.	×	×	×	×				×							
η	hcp	×		×			×				×					
μ	rhomb.							×	×							
Laves	hexagonal		×		×		×		×		×				×	
M_3B_2	tetrag.			×	×	×				×	×			×		
MN	cubic			×	×		×				×					

Ni-based superalloy castings intended for hot sections in aircraft applications are produced by investment casting under vacuum to avoid oxidation of reactive elements. This technique uses a pattern made from wax or plastic, which is allowed to harden into a mold shell. The pattern is then removed typically by steam, after which, the raw material, which has been produced by vacuum induction melting

(VIM) is poured into the mold shell, and allowed to solidify. Finally, the mold is destroyed to recover the casting [12, 13]. Subsequently, HIP is performed to close any micro-shrinkages from the casting process, and at the same time, to level out any micro-segregation.

2.1. Alloy 718

Alloy 718 is an Fe–Ni-based superalloy, which was developed in the 1960s by Eiselstein [1] to provide a material free from strain age cracking, which as mentioned earlier, is a solid-state cracking phenomenon occurring in the HAZ during the post-weld heat treatment. The alloy has an austenitic matrix with the addition of several elements, which contribute to its mechanical properties. Nb has an important role, as it aids the formation of several phases such as γ´´, δ, Laves, and MC carbides. γ´´ is a metastable phase, which confers on the alloy its strength up to 650 °C. Above this temperature or during long exposure times, γ´´ transforms into δ, leading to a deterioration of the mechanical properties. The δ phase precipitation in the temperature range of 870–950 °C is used for grain size control. The Laves phase is often considered detrimental to the mechanical properties of the alloy owing to its brittle characteristics [12, 14, 15]. The pre-weld homogenization heat treatments or HIP treatments are performed to dissolve the Laves phase with a view to minimizing the extent of cracking during welding. The commonly used solution heat treatment at 1050 °C cannot dissolve the detrimental Laves phase. Therefore, homogenization heat treatments at higher temperatures have been developed in the industry. Two main HIP treatments from the aerospace industry have been developed by General Electric Aviation (GEA) and Pratt & Whitney (P&W). They consist of heat treating the material at 1120 °C [9] and 1190 °C [10, 11], which are, respectively, below and above the incipient melting temperature of the Laves phase.

2.2. ATI 718Plus

A higher temperature stability was achieved for ATI 718Plus by substituting the metastable γ´´ by the more stable γ´ strengthening phase, and by carefully selecting an Al/Ti ratio that delayed the transformation of γ´ to η. The higher thermal stability of the strengthening phase led to an operating temperature of 50 °C higher than that of Alloy 718 [3]. A cast version was developed under the Metals Affordability Initiative (MAI) program [5]. Apart from the primary strengthening phase, the material has similarities to Alloy 718 with regard to the solidification range and microstructural features [16, 17]. Similar to Alloy 718, the γ/Laves eutectic reaction occurs at 1160 °C. Homogenization heat treatments above 1100 °C are required to dissolve the Laves phase [18].

2.3. Haynes 282

Haynes 282 is a γ´ precipitation hardening Ni-based superalloy, which can be used in the temperature range of 650–900 °C. The high-temperature performance was achieved by a careful balance of the γ´ phase fraction [4]. Contrary to Alloy 718 and ATI 718Plus, Haynes 282 is devoid of the low-melting

Laves phase. Its microstructural features include primary Ti–Mo-rich MC carbides, secondary carbides (e.g., $M_{23}C_6$, M_6C, Mo-rich borides), and the σ phase [19–21]. The recommended solution heat treatment for the alloy is between 1120–1150 °C, which is the temperature range required for the dissolution of secondary carbides [4, 22].

3. Hot cracking in superalloys

Hot cracks are the ones that occur during welding owing to the presence of liquid in the microstructure, and are divided between the cracking occurring in the fusion zone (FZ) and the HAZ. These are named solidification and HAZ liquation cracks, respectively. The prominent theories that explain the phenomenon of hot cracking are summarized below.

3.1. Solidification cracking

Pumphrey et al. [23] proposed the so-called "shrinkage brittleness theory" to explain the cracking mechanism during casting and welding of aluminum. It was postulated that a brittle temperature range (BTR) exists, in which the material is susceptible to cracking owing to the lower ductility conferred by the presence of the liquid phase. This BTR has an upper limit termed "coherent temperature", which is the temperature at which growing dendrites come into mutual contact by forming a solid-coherent network; on the other hand, the lower limit is defined by the solidus temperature. The BTR range is primarily influenced by the composition of the alloy.

Pellini [24] formulated the "strain theory" based on his investigations on hot tearing in castings, and later adapted the same to welding as well. The strain theory presumes the presence of liquid films close to the solidus temperature. Their presence at the grain boundaries is the main cause of the reduced ductility owing to the low stress required for a film separation. According to the strain theory, hot cracks cannot form in the so-called mushy zone, because of the ability of the liquid to flow and heal the cracks.

The "generalized theory" by Borland [25], depicted in Figure 1, combines the previously mentioned theories, although with some modifications. Firstly, Borland separates the solidification range into four stages, as described below:

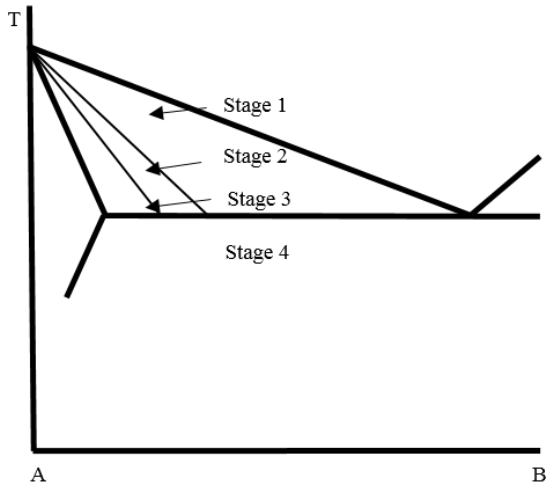

Figure 1. Solidification stages according to Borland´s generalized theory; adapted from [25].

Stage 1: primary dendrites form as the temperature drops below the liquidus temperature.

Stage 2: the dendrites interlock by forming a solid network. In this stage, only the liquid is capable of moving between the dendrites.

Stage 3: the grain development occurs. Here, the liquid is not capable of free movement as it is hindered by the continuous network.

Stage 4: all the liquid solidifies.

According to Borland, cracks can form in Stage 2 once an "almost continuous" network of dendrites has formed. In this stage, healing is possible, as there is sufficient amount of liquid, which can backfill the incipient cracks. He also defined a "critical solidification range" (CSR), associated with Stage 3, wherein significant cracking can occur, as the confinement of liquid to inter-dendritic areas without the ability to move freely occurs. This in turn, inhibits the healing of cracks. A wider CSR promotes a larger temperature range over which the liquid is present, and hence the susceptibility to cracking increases. In Stage 4, cracking no longer occurs, as the material is fully solidified.

Matsuda et al. [26] proposed a modified concept of solidification cracking in reference to Borland´s "generalized theory", based on experiments, which allowed a direct observation of the cracking of welds through a high speed camera. Based on their observations, Stages 1 and 2 defined by Borland, were shifted towards the liquidus. Moreover, Stage 3 was divided into a "film stage" 3(h) and "droplet stage" 3(l), as depicted in Figure 2. Crack initiation can occur in the liquid film stage and propagate in the droplet stage; however, initiation is not possible in the latter owing to the extensive solid–solid bridging.

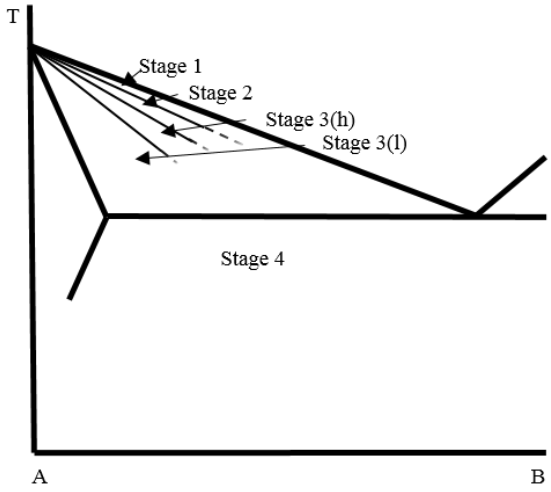

Figure 2. Solidification stages according to Matsuda et al.; adapted from [26].

All the theories agree upon the fact that weld solidification cracking originates from a combination of metallurgical factors and local strains at the final stages of solidification in the presence of some liquid

phase along the solidification boundaries. The solidification range is considered among the most important factors in determining the susceptibility to solidification cracking. Generally, the lower the solidification temperature, the wider the temperature range, at which the liquid will exist, and this can aggravate the cracking tendency [27, 28]. Other important metallurgical factors are the amount and distribution of liquid at the final stages of solidification and grain boundary wetting. Cracking is enhanced when the surface tension of the liquid is low and continuous thin liquid films wet the grain boundaries. When a sufficient amount of terminal liquid is present, the liquid has the ability to flow back into the cracks and heal them. The backfilling effect is especially relevant in alloys, such as-cast Alloy 718 and cast ATI 718Plus, which solidify by a eutectic reaction. The solidification sequence in Nb-bearing alloys terminates with the following eutectic reaction [29]:

$$L \rightarrow (\gamma + \text{Laves})$$

The γ/Laves eutectic reaction occurs at a temperature below the solidus of the γ phase; thus, it is responsible for extending the solidification range. The solidification range values obtained by JMatPro (liquid fraction at 0.01 wt.%) and experimental values by differential scanning calorimetry (DSC) for three alloys are summarized in Table 2. Alloy 718 and ATI 718Plus have a similar solidus temperature and solidification range of approximately 1160 and 170 °C, respectively, whereas Haynes 282 has a higher solidus of approximately 1240 °C and a shorter solidification temperature range of 120 °C. Generally, larger solidification range temperatures were predicted by simulations than the experiments. Figure 3 shows an example of a solidification crack in ATI 718Plus, surrounded by γ-Laves eutectic constituents.

Table 2. Solidification temperature ranges (°C) for cast Alloy 718, ATI 718Plus, and Haynes 282.

	JMatPro		**DSC**			
	$T_{liquidus}$	$T_{solidus}$	Sol. Range	$T_{liquidus}$	$T_{solidus}$	Sol. range
Alloy 718	1357	1095	262	1334 [6]	1157 [6]	177 [6]
ATI 718 Plus	1328	1110	218	1328	1162	166
Haynes 282	1350	1175	175	1360 [30]	1244 [30]	116 [30]

There are two points of view on the effect of the base metal condition on the susceptibility to solidification cracking. It is believed that melting and solidification in the FZ eliminates the thermal history of the alloy [31], which makes the solidification cracking independent of the base metal condition. On the other hand, it is also believed that the weld metal grain size is a function of the base metal grain size owing to the epitaxial growth, which consequently, can influence the susceptibility towards cracking [32]. Fine weld grain structure is considered less susceptible to cracking than coarse

grain structure owing to its better accommodation of the strain [28]. The weld pool shape is also considered to be an important factor. When welding at a high speed, centerline cracks can form owing to the tear-shaped weld pool; these cracks create an abrupt angle with the columnar grains forming from the two sides of the fusion line. This is not a concern when welding at low speeds because the elliptical-shaped welds lead to a smooth transition of the columnar grains at the weld center [27].

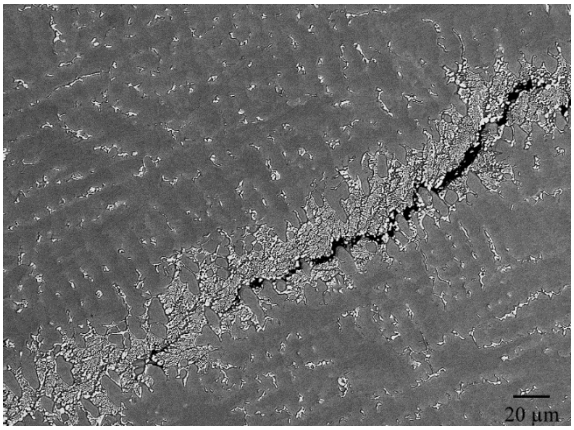

Figure 3. Solidification crack surrounded by γ/Laves eutectic in cast ATI 718Plus [33].

3.2. HAZ liquation cracking

The mechanisms associated with the formation of HAZ liquation cracks are referred to as "liquation". The formation of liquid films at the grain boundaries locally lower the ductility and therefore, increase the susceptibility to cracking. The phases or segregating elements responsible for the crack formation vary from one alloy to another.

The liquation of the grain boundaries leading to HAZ cracking can occur in two ways — segregation mechanism and penetration mechanism. The segregation mechanism occurs when solute or impurity elements segregate at the grain boundaries by diffusion to suppress the local melting temperature, thus leading to grain boundary melting. The presence of P, S, and B at the grain boundaries is known to promote liquation cracking in Ni-based superalloys. The segregation of B may occur in two ways, namely via equilibrium and non-equilibrium mechanisms. The equilibrium segregation decreases as the temperature increases because of the higher diffusion. On the other hand, the non-equilibrium segregation occurs during cooling from high temperatures from the diffusion of the vacancy-solute complexes to the grain boundaries, where the solute atoms are deposited. The extent of non-equilibrium segregation increases with temperature, as the concentration of the vacancies also increases [34–36]. In the penetration mechanism, the cracking occurs when a moving grain boundary intersects a locally melted region. The penetration mechanism is possible in two ways, by constitutional liquation and eutectic melting [28, 37]. The constitutional liquation mechanism was proposed by Pepe and Savage [38] for "maraging steel" weldments. Here, a key factor is that the particles do not dissolve completely

under the non-equilibrium conditions generated by the rapid heating during the welding. A diffusion gradient is generated at the particle–matrix interface, which partially dissolves the precipitate and creates a solute-enriched area. Liquid forms, once a local eutectic composition is reached. This mechanism was reported in Nb-bearing superalloys, as well as in other precipitation hardening Ni-based superalloys [39–41]. A schematic drawing illustrating this mechanism is shown in Figure 4. Next, Figure 5 shows a scanning electron microscope (SEM) image of a constitutionally liquated carbide in the HAZ of cast ATI 718Plus.

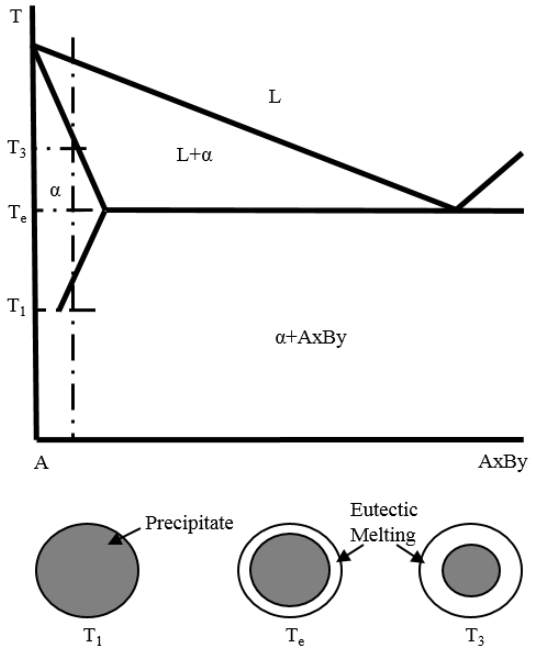

Figure 4. Schematic diagram depicting the phase change and constitutional liquation; adapted from [38].

According to Weiss and Grotcke [42], constitutional liquation is function of the interaction among the following:

- Heating rate
- Kinetics of dissolution of precipitates
- Minimum solidus temperature
- Homogenization of the elements from the precipitate into the matrix

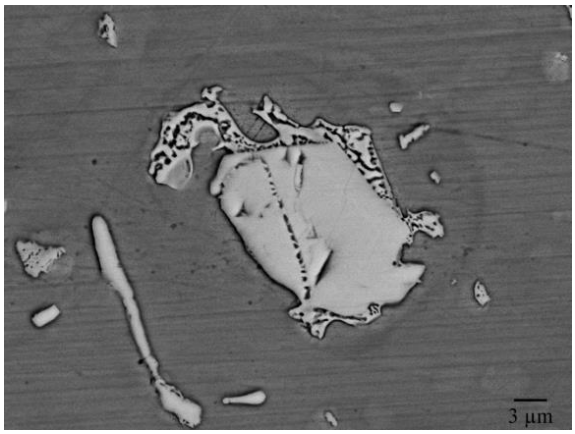

Figure 5. Constitutional liquation of NbC in cast ATI 718Plus.

Another liquation mechanism, which is common in cast materials is via eutectic melting. In contrast to the constitutional liquation mechanism, wherein no precipitate melting occurs, here, eutectic melting occurs along the inter-dendritic regions, which have a lower melting temperature than the surrounding matrix [28, 37].

The following are the liquation mechanisms reported for Ni-based superalloys [6, 38, 43]:

- Constitutional liquation of secondary phases
- Melting of the matrix
- Liquation of precipitation hardening phases in high-volume fraction γ´ alloys
- Melting of residual eutectic in cast material
- Liquation from solute segregation

The Laves phase has been considered a major cause for the HAZ liquation cracking in cast Alloy 718 [7, 44, 45]. The segregation of minor elements along the grain boundaries constitutes another detrimental effect on the HAZ liquation cracking susceptibility. Elements, such as S, P, and B have been reported to be detrimental to the HAZ liquation cracking susceptibility [44, 46–50]. Especially, B is known to be a melting point depressant element that lowers the liquation temperature below the equilibrium of the solidus. Moreover, it has the ability to improve the wetting characteristics of the liquid along the grain boundary, thus favoring its distribution.

The recently developed cast ATI 718Plus has similarities with Alloy 718; however, there is a lack of literature concerning its weldability. A weld repair study on cast ATI 718Plus reported the most homogenized material condition (Laves-free) to be more crack-susceptible than a moderately homogenized condition [18]. Nonetheless, a majority of the studies have covered the weldability of wrought ATI 718Plus only. The wrought version is devoid of the Laves phase, which is often found in

as-cast materials. The segregation of P and B along the grain boundaries has been reported to aid in the HAZ liquation cracking [51, 52].

Similar to the case of ATI 718Plus, very little is known regarding the weldability of the recently developed cast Haynes 282. Although the wrought material was reported to have a good weldability [19, 53, 54], B-segregation at the grain boundaries was reported to be detrimental to the HAZ liquation cracking [20, 30].

Careful control of the grain size is one very important tool for controlling the mechanical properties of superalloys. While a large grain size is considered beneficial for creep strength, a small grain size is considered beneficial in respect of tensile and fatigue properties; furthermore, it also has a positive effect on the weldability, as a small grain size provides a larger area for stress accommodation [28, 55, 56]. Therefore, the grain size should be carefully controlled according to the specific application. In wrought materials this is preferably done by precipitating η or δ phase along the grain boundaries, which provides a grain size in the range of 10 to 200 μm [57]. However, in castings, the grain size can reach up to 3 mm [58]. One way to keep a small grain size is by utilizing the Microcast-X process through a careful control of the pouring temperature and induced turbulence in the molten metal [12], which can yield grain sizes in the range of 90–1600 μm, (significantly lower than conventional castings [58]).

4. Weldability tests for hot cracking

Weldability tests can be classified into simulative and self-restraint tests. The simulative weldability tests were used in the current study. They provide a better reproduction of welding conditions under a controlled parameter set and allow quantification of the cracking extent. The self-restraint tests are used for qualitative analysis and provide an indication of the material's vulnerability to cracking [37, 59].

4.1. Varestraint testing

The Varestraint (variable-restraint) testing was first developed by Savage and Lundin in the 1960´s at the Rensselaer Polytechnic Institute [60]. The first configuration applied longitudinal bending to the length of the test plate. This type of test (longitudinal type) produces cracking both in the FZ and HAZ. Later on, variants applying welds transverse to the sample length (transverse-Varestraint) and using a spot (spot-Varestraint) tests were developed to separate the FZ and HAZ cracks, respectively. A schematic diagram of the tests is shown in Figure 6. The augmented strain can be controlled using interchangeable die blocks. The extent of the strain at the welded surface can be obtained by:

$$\varepsilon = \frac{t}{2R} \qquad \text{Eq.1}$$

where *t* is the sample thickness and *R* is the radius of the die block.

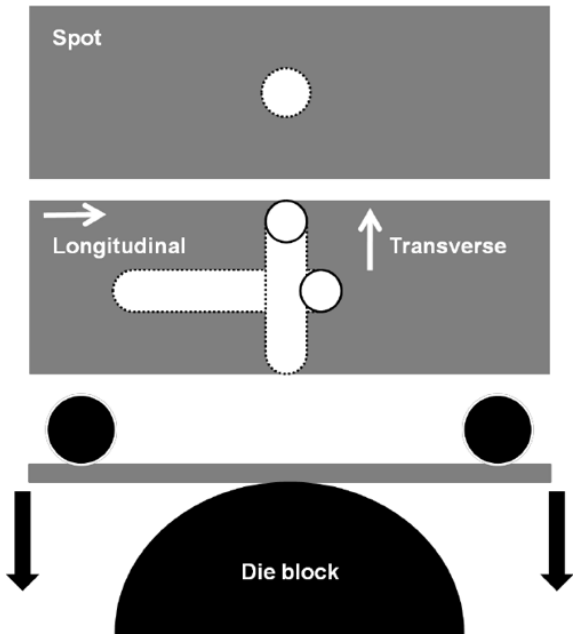

Figure 6. Schematic diagram of different types of Varestraint tests [6].

Crack measurements are generally performed under a stereomicroscope at a magnification between 20–50x. Different approaches are used for crack evaluation. Several metrics have been traditionally used

for quantifying the cracking susceptibility, and these are summarized in Table 3. The total crack length (TCL), which is the sum of the lengths of all the cracks and the average TCL (Avg. TCL) are commonly used. The maximum crack length (MCL) or the maximum crack distance (MCD) is used for evaluating the BTR or the solidification cracking temperature range. The threshold strain is the minimum strain required for cracking, whereas the saturation strain is the strain, above which the crack length does not increase [37].

Table 3. Commonly used parameters for crack evaluation.

Parameter	References
TCL	[61–65]
Avg. TCL	[33, 41, 66]
MCL	[63, 67]
MCD/SCTR	[68, 69]
Threshold strain	[28]
Saturation strain	[28, 37]

The setup of the Varestraint test used in the current study is shown in Figure 7.

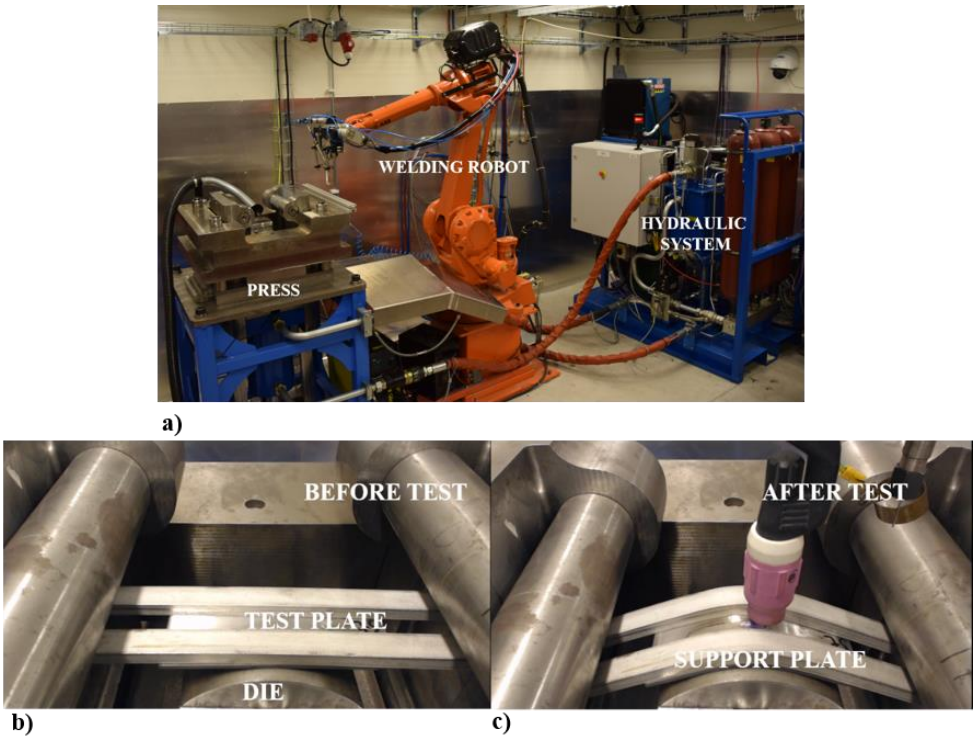

Figure 7. Varestraint weldability testing equipment at University West; setup a) before and b) after the test.

4.2. Gleeble testing

The Gleeble thermal-mechanical simulator was developed in the 1950s at the Rensselaer Polytechnic Institute [70]. The Gleeble test uses a resistance heating to heat the samples and water cooled grips (usually made from Copper) for cooling by conduction. This machine is capable of providing a heating rate of up to 10,000 °C/s and an accelerated cooling with quenching systems. The Gleeble 3800 system used in the current study is shown in Figure 8.

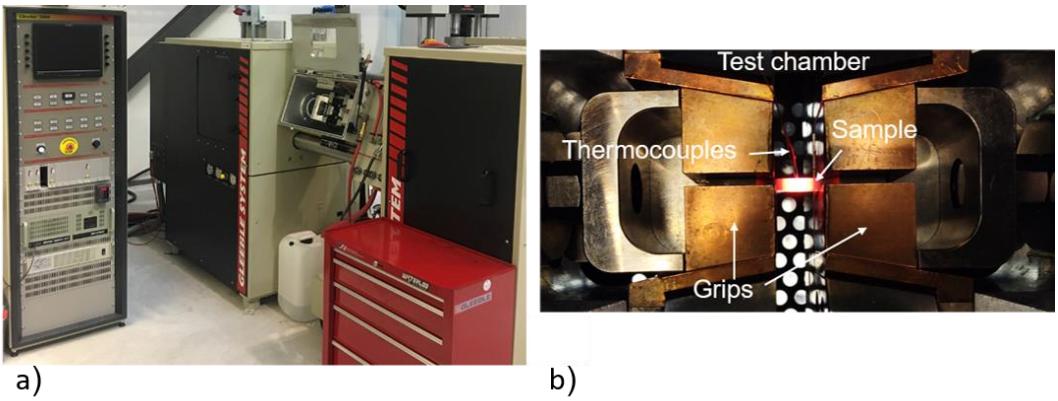

Figure 8. a) Gleeble 3800 system at University West; b) test setup showing sample heating in between the copper grips and the attached thermocouples.

In the hot ductility test (HDT), the ductility of a specimen is measured in terms of its area reduction by pulling the material at on-heating and on-cooling weld thermal cycles. The rapid ductility drop during heating indicates the onset of liquation, which causes grain boundary embrittlement. The temperature at which the ductility drops to zero is referred to as nil ductility temperature (NDT). The on-cooling test is performed by heating up to a peak temperature (T_P), which leads to an appreciable melting, but below the liquidus temperature (T_L). Generally, a peak temperature (T_P) is chosen between the NDT and the nil strength temperature (NST). During the on-cooling, the BTR is measured as the difference between T_P and the ductility recovery temperature (DRT), for which 5 % ductility recovery is achieved [37, 71]. A typical hot ductility curve with the important points highlighted is shown in Figure 9.

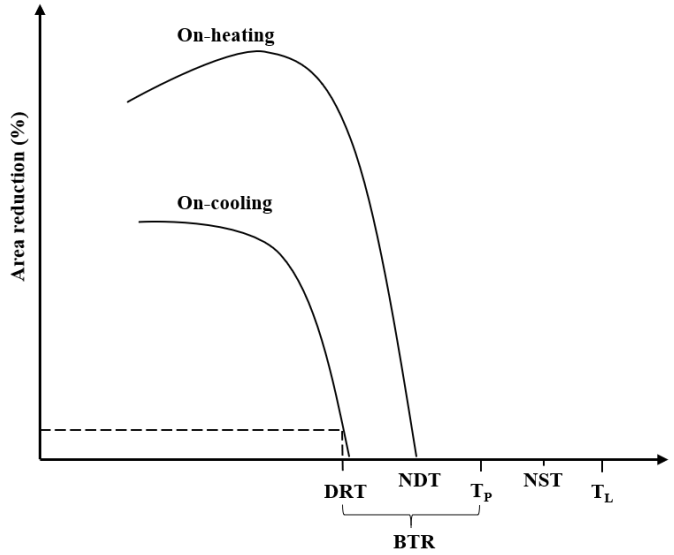

Figure 9. A schematic diagram of typical hot ductility signature with weldability parameters used in this study.

5. Experimental methods

5.1 Materials and heat treatments

The chemical compositions of cast superalloys Alloy 718, ATI 718Plus, and Haynes 282 are summarized in Table 4.

Table 4. Compositions in wt.% of cast Alloy 718 (Papers I and II), ATI 718Plus (Papers III and IV), and Haynes 282 (Paper V).

Element	Alloy 718	ATI 718 Plus	Haynes 282
Ni	52.98	Balanced	Balanced
Cr	18.11	20.5	19.3
Fe	Bal.	9.7	0.2
Co	0.07	8.3	9.9
Nb	5.31	6.3	0.1
Mo	2.98	2.7	8.5
Al	0.42	1.5	1.44
Ti	0.99	0.8	2.07
C	0.05	0.05	0.05
W	0.01	1.0	0.1
Mn	0.03	0.01	0.1
Cu	0.01	0.1	0.1
Si	0.07	0.03	0.001
P	0.009	0.008	0.004
B	0.03	0.005	0.006
Ta	–	–	0.1
S	–	–	0.001

Table 5 summarizes the heat treatments employed in this study. Alloy 718 was subjected to HIP at 1120 °C/4 h at 100 MPa to partially dissolve the Laves phase, followed by a post-HIP in vacuum at 1050 °C, to dissolve any γ´´ precipitated during the cooling. A second variant of HIP was applied at 1190 °C/4 h at 100 MPa to put the Laves phase in a solid solution, followed by a post-HIP in vacuum at 870 °C /10 h to precipitate the δ phase. A common solution heat treatment at 950 °C/1 h was applied after each post-HIP step. Cast ATI 718Plus was subjected to three homogenization heat treatment temperatures at 1120, 1160 and 1190 °C with a dwell time of 4 h. Cast ATI 718Plus has higher Nb content than cast Alloy 718. Therefore, a higher amount of Laves phase is expected in the “as-cast” condition. Additional

heat treatment trials at 24 h dwell times were applied to evaluate the homogenization effect. Cast Haynes 282 was subjected to three homogenization heat treatments at 1120, 1160, and 1190 °C/4 h, respectively, followed by an additional heat treatment at 1135 °C/ 0.5 h to precipitate the secondary carbides along the grain boundaries. The pseudo-HIP for cast ATI 718Plus and Haynes 282 were performed in laboratory furnaces at the ambient pressure, followed by water quenching to avoid the precipitation of γ′ phase.

Table 5. Heat treatment steps for cast Alloy 718, ATI 718Plus, and Haynes 282.

Material	HIP/pseudo-HIP
Alloy 718	HIP at 1120 °C/4 h + Post-HIP at 1050 °C/1 h + FC to 650 °C in 1 h + SHT at 950 °C/1 h + AC
	HIP at 1190 °C/4 h + Post-HIP at 870 °C /10 h + FC to 650 °C in 1 h + 950 °C/1 h + AC
ATI 718Plus	1120 °C/4 h and 24 h + WQ
	1160 °C/4 h + WQ
	1190 °C/4 h and 24 h + WQ
Haynes 282	1120 °C/4 h + 1135 °C/0.5 h + WQ
	1160 °C/4 h + 1135 °C/0.5 h + WQ
	1190 °C/4 h + 1135 °C/0.5 h + WQ

FC: furnace cooling, AC: air cooling, WQ: water quenching

5.2. Varestraint weldability testing

Cast plates were electric discharge machined into test plates with approximate dimensions of 150 × 60 × 3.3 mm^3 for the Varestraint testing. Bead-on-plate welding was performed longitudinal to the bending direction at various test radii from 20 to 200 mm, which corresponded to the augmented strain levels of 0.8%, 1.1%, 1.6%, 2.1%, 2.7%, 3.3%, 3.9%, and 8.2%, respectively. The test parameters for the Varestraint testing and Gas tungsten arc welding (GTAW) are summarized in Table 6. The parameter selection was based on a previous DOE (design of experiments) study involving Varestraint tests, which produced the least amount of scatter [72].

Table 6. Parameters used for longitudinal Varestraint weldability testing using GTAW.

Welding speed (mm/s)	Stroke rate (mm/s)	Weld current (A)	Arc length (mm)	Ar gas flow (l/min)
1	10	70	2	15

For the research reported in **Paper I (Alloy 718)**, seven plates for each condition and strain level were tested, i.e., a total of 168 test plates. **Paper II (ATI 718Plus)** reported on the tests performed at strain levels of 1.1%, 1.6%, 2.1%, and 2.7%, with three test plates for each strain level and condition, i.e., a total of 72 test plates. In **Paper V (Haynes 282)**, testing was reported at strain levels of 1.1%, 1.6% and 2.7%, with three test plates for each strain level, i.e., a total of 36 test plates.

Following the testing, the oxide layer from the welding was removed using a fine abrasive paper. Crack measurements were performed using stereomicroscope at 20–50x magnification and crack lengths were recorded for FZ and HAZ. The Avg. TCL values were plotted against the augmented strain for evaluation.

5.3. Gleeble testing

Investment cast plates with dimensions of 300 × 60 × 12 mm^3 were cut out to final dimensions using abrasive water jet cutting. The cast plates are as shown in Figure 10.

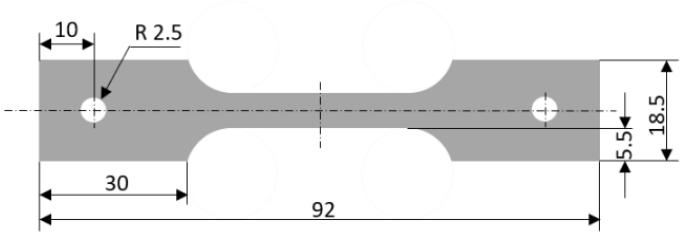

Figure 10. Sample geometry used for hot ductility tests; sample thickness: 3.5 mm.

The test samples were heated at a rate of 111 °C/s to various test temperatures, maintained at the specific temperature for 0.03 s, and pulled to fracture at a stroke rate of 55 mm/s, according to the details provided in Table 7. The NST temperature was determined by heating the sample and applying a load of approximately 100 N until it fractured. The NST values were determined only for Alloy 718 and ATI 718Plus, as very limited amount of test samples were available for Haynes 282. A common peak temperature of 1220 °C was selected for comparison among the three alloys. On-heating and on-cooling ductility values were measured in terms of the area reduction and plotted against the temperature for evaluation.

Table 7. Test parameters used for Gleeble testing.

Heating rate	Cooling rate	Peak temp.	Stroke rate	Holding time	Free-span
111 °C/s	50 °C/s	1220 °C	55 mm/s	0.03 s	20 mm

5.4. Sample preparation and characterization

5.4.1 Metallographic preparation

Base metal and weld cross-sections were cut out from the Varestraint and Gleeble tested samples. The metallographic preparation steps are summarized as follows:

- Mounting using conductive and thermoplastic compounds with Buehler SimpliMet 2000
- Grinding steps of 125 and 45 µm discs with Buehler PowerPro 5000
- Polishing steps with a Buehler Hercules S rigid disc using a 9-µm Kemet liquid diamond, and with a Trident cloth disc using a 3-µm Kemet liquid diamond
- Electrolytic etching using oxalic acid at 3.2 V for approximately 10 s

5.4.2 Grain size evaluation

Grain size analyses were carried out according to ASTM E112 standard [73]. The grain size measurements for the cast Alloy 718 followed the metallographic steps previously described with the only difference being the type of etchant used. Kalling´s 2 (2 g $CuCl_2$, 49 mL HCL, 40-80 mL ethanol) was used for the grain size evaluation. For cast ATI 718Plus and Haynes 282, the grain size evaluation was conducted on macro-etched samples with 90% HCL, 10% HNO_3, and 120 g/L $FeCl_3$, powder heated to approximately 50 °C.

5.4.3 Microstructural characterization

Microstructural characterization was conducted using an Olympus BX60M optical microscope and a LEO 1550 FEG-SEM with Oxford electron dispersive X-ray spectroscopy.

5.4.4 SIMS and NanoSIMS analysis

Papers II and **IV** describe the time of flight-second ion mass spectrometry (ToF-SIMS) analysis performed for detecting the segregation of minor elements at the grain boundaries using a TOF.SIMS 5 instrument, with a 25 kV Bi cluster ion gun as the primary ion source, and a 10 KV Cs ion source for sputtering. The samples were analyzed using a pulsed primary ion beam (Bi_3^+ at 0.2 pA) in delayed extraction mode, with a focus of approximately 400 nm. All the spectra were acquired and processed with the Surface Lab software. The spectra were internally calibrated to signals of C^+, CH_2^+, CH_3^+, and Cr^+ for the positive ion mode, and C^-, CH^-, C_2^-, and Si^- for the negative ion mode. The samples were etched using a C_s^+ beam at 20 nA/3KV.

Paper V reported on the examination of the grain boundary segregation by a CAMECA NanoSIMS50L secondary ion mass spectrometer, using a primary beam of Cs^+. The mass-resolved images were obtained for $^{11}B^-$, $^{12}C_2^-$, $^{28}Si^-$, $^{31}P^-$, and $^{11}B^{16}O_2^-$.

5.4.5 Hardness testing

The hardness measurements were conducted using a Shimadzu HMV-2 micro-hardness testing machine with a force of 0.5 Kgf (HV0.5) and a holding time of 10 s.

5.4.6 DSC

DSC was performed using a Netzsch-STA 441 F1 Jupiter® simultaneous DSC-TG equipment using heating and cooling rates of 10 °C/min at a soak temperature of 1400 °C.

5.4.7 Material modeling

JMatPro 11.0, in conjunction with an Ni-based superalloy database was used to model the phase stability of the investigated alloys.

6. Results and Discussion

6.1. Alloy 718 (Papers I and II)

The effect of HIP-1120 was to partially dissolve the Laves phase, with the volume fraction of the secondary precipitates decreasing from approximately 3.7% in the as-cast condition to approximately 1.7%, as shown in Figures 11 and 12. After being exposed to HIP-1190, the Laves phase was completely dissolved, with the MC carbides remaining, and significant δ phase precipitation surrounding the carbides, as well as at the grain boundaries, with total of 1.3 vol.% of the secondary precipitates. Here, the phase fraction was measured in area percentage and assumed to be the same as the volume fraction percentage. The hardness decreased slightly from an initial value of 260 HV in the as-cast condition to 210-220 HV after HIP, whereas significant grain growth occurred from 1.7, 2.6, and 3.3 mm in the as-cast, HIP-1120, and HIP-1190, respectively, as shown in Figure 12.

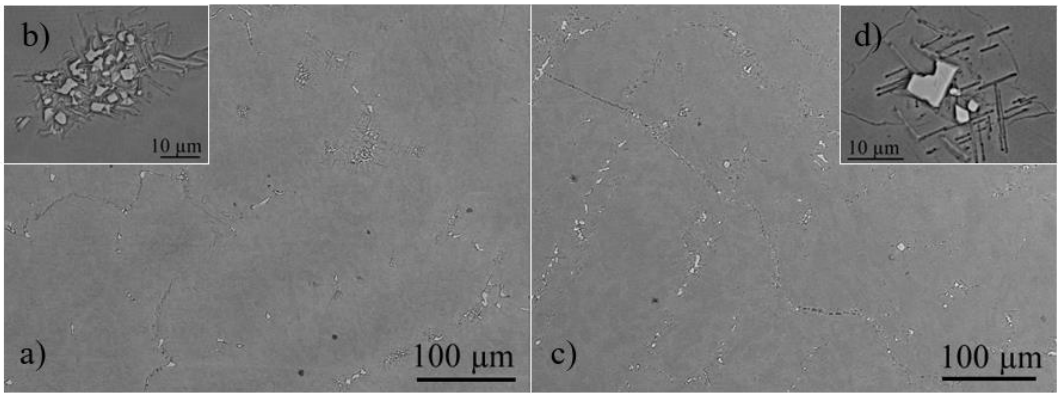

Figure 11. SEM-backscattered images showing the effect of HIP: a) after HIP-1120; b) partially dissolved Laves phase; c, d) after HIP-1190 showing the presence of NbC carbides and δ phase.

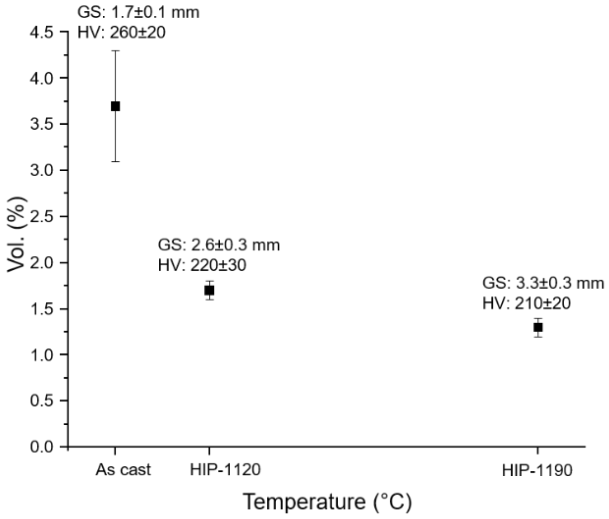

Figure 12. Volume fraction of the secondary precipitates, hardness, and grain size in as-cast, HIP-1120, and HIP-1190.

SIMS analysis revealed minor elements, such as C, Si, P, S, and B segregated to different extents along the grain boundaries. The elemental map for HIP-1190 of Alloy 718 is shown in Figure 13.

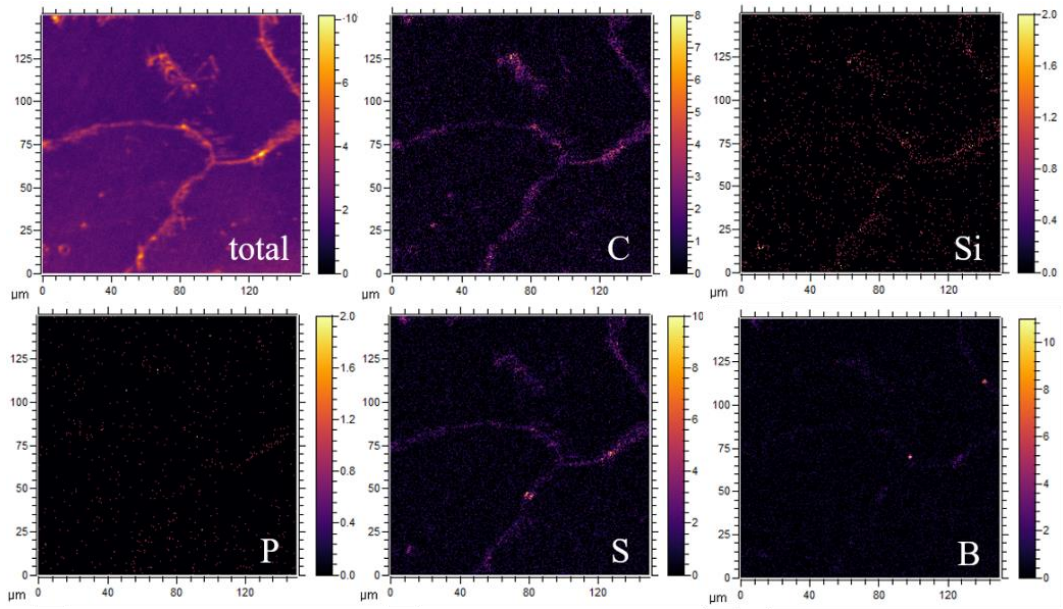

Figure 13. SIMS map showing segregation of minor elements along the grain boundaries at HIP-1190 of Alloy 718.

After the Varestraint testing, a wide scatter in the Avg. TCL values was found for both solidification cracking and HAZ liquation cracking, as shown in Figure 14 a) and b). Despite the large scatter in the results, which is typical of cast materials, the overall conclusion was that there were no differences in the solidification cracking susceptibility in different base metal conditions. The HAZ liquation cracking,

on the other hand, revealed that the as-cast condition exhibited the least amount of cracking, followed by HIP-1120, and HIP-1190.

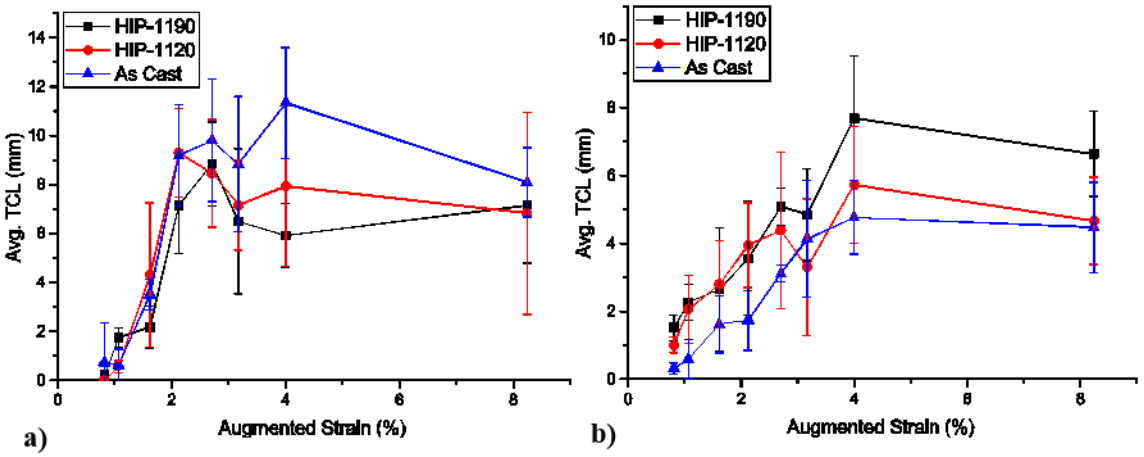

Figure 14. Variation in the Avg. TCL with standard deviations for the as-cast, HIP-1120, and HIP-1190 conditions: a) FZ; b) HAZ.

Small and disconnected cracks associated with the melting of the γ/Laves eutectic phase were found in the as-cast condition (Figure 15), while in the HIP'ed conditions, the cracking occurred along the grain boundaries. In particular, the grain size increase allowed the cracks to propagate longer than in the lower grain size condition as shown in Figure 15. A larger grain size is generally known to be detrimental in terms of hot cracking susceptibility [28, 55, 56, 74], and this was found to be an important factor in differentiating the cracking susceptibility among the HIP'ed conditions.

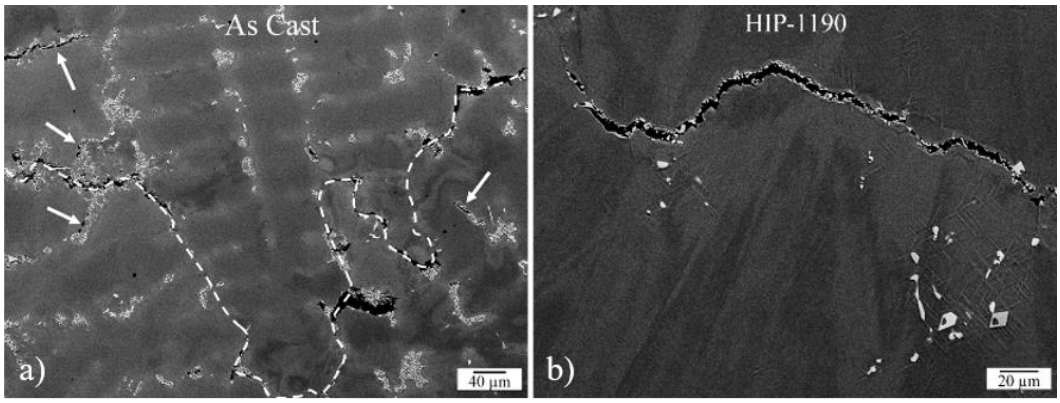

Figure 15. a) Cracks formed in the liquated regions in the as-cast condition; b) liquation cracking in the HIP-1190 condition of cast Alloy 718.

After the hot ductility tests, HIP-1120 exhibited on-heating ductility of approximately 50 % at 950 °C and experienced a steep decrease above 1100 °C, whereas HIP-1190 exhibited a rather low ductility, considering a significant scatter between the tests. The ductility drop for HIP-1190 started slightly above 1050 °C. The NDT for both the conditions was recorded at 1150 °C, as shown in Figure 16 and presented

in Table 8. An on-cooling ductility recovery of 5% occurred at 1130 °C for HIP-1120 and 1115 °C for HIP-1190, with corresponding BTRs of 90 and 105 °C, respectively.

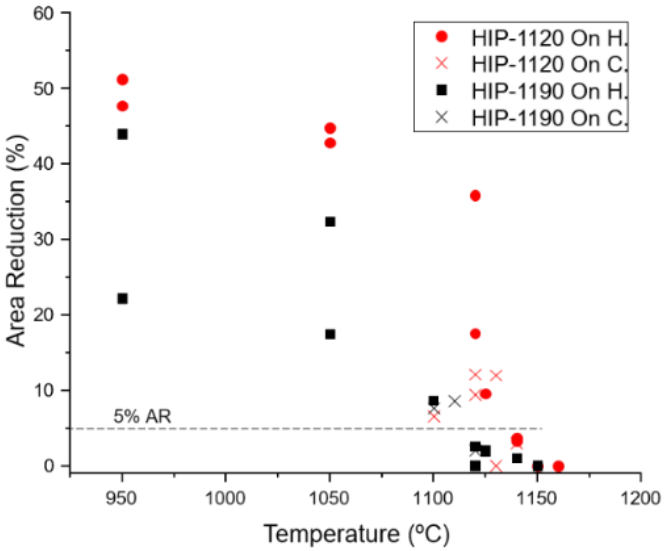

Figure 16. On-heating (On H.) and on-cooling (On C.) signatures after the Gleeble testing.

Table 8. Summary of different weldability parameters of Alloy 718; all the temperatures are in °C.

Condition	NST	NDT	DRT	BTR
HIP-1120	1270	1150	1130	90
HIP-1190	1255	1150	1115	105

A relatively rapid ductility recovery occurred in HIP-1120 owing to the limited amount of melting, which was confined to liquation of Laves phase in the inter-dendritic regions, and partially from grain boundary melting, as shown in Figure 17 a). The extent of liquation was more severe for HIP-1190, as evident from Figure 17 b). Large MC carbides were seen to be unaffected in both the HIP conditions, whereas small carbides with constitutional liquation in HIP-1190, as pointed by an arrow. The extensive melting reflected in a larger BTR of 105 °C, indicating the temperature range, where the material is in partial liquid form, which was 15 °C wider than that for HIP-1120.

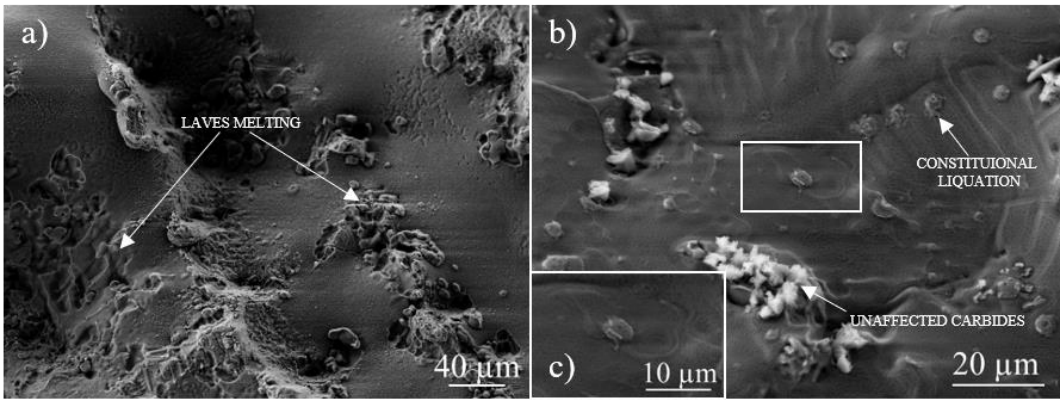

Figure 17. Fracture surfaces: a) HIP-1120 pulled to fracture at 1130 °C with inter-dendritic liquid from liquation of Laves; b) HIP-1190 at 1130 °C with grain boundary melting and small carbides undergoing constitutional liquation.

The ductility drop below the solidus of the alloy is believed to have occurred through liquation of solute segregation of S, P, and B, which are known to lower the liquation temperature of the grain boundaries. During the on-cooling, these elements extended the solidification range below the equilibrium solidus of the alloy [44, 49, 50, 75, 76]. Figure 18 shows the effect of Nb as a solute element on the solidus of the alloy. With the core compositions highlighted in the diagram, the supersolidus melting appears to be much severer in the HIP-1190, where a more extensive homogenization raised the Nb content at the cores, compared to that in HIP-1120. Therefore, both Nb and the minor elements influenced the grain boundary liquation, with more extensive liquation in HIP-1190, and a larger grain size contributing to the higher HAZ liquation cracking susceptibility.

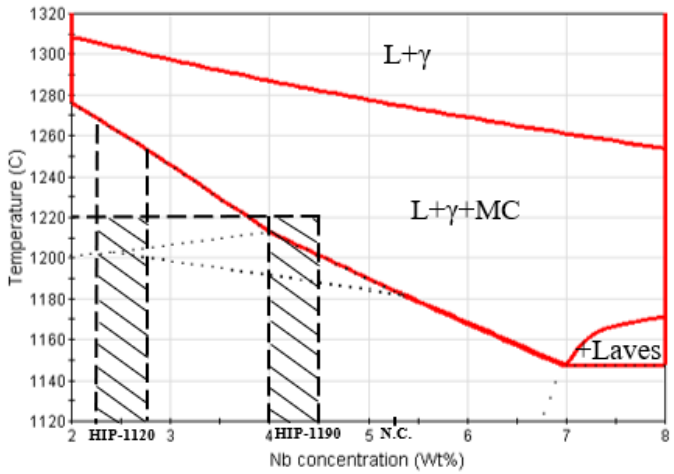

Figure 18. JMatPro isopleth diagram showing the variation in the solidus temperature with variation in the Nb concentration (Ni balance), with highlighted compositions in the two HIP homogenization treatments and reference nominal composition (N.C.) in the alloy.

6.2. ATI 718Plus (Papers III and IV)

The effect of homogenization heat treatments on ATI 718Plus is shown in Figure 19. All the heat treatments except for 1120 °C/4 h, were able to dissolve the Laves phase. The partial dissolution of Laves occurred at 1120 °C/4 h. The heat treatment at 1190 °C/4 h also exhibited melting of the MC carbides. The area fraction of the secondary phases in the inter-dendritic areas were estimated to be approximately 5.3% in the as-cast condition, 2.6% at 1120 °C/4 h, and 0.5 wt.% in the other conditions, which were able to dissolve most of the Laves phase. The base metal hardness decreased from the initial value of approximately 410 to 330–350 HV after the homogenization heat treatments. The grain size with an average value of approximately 1.3 mm was similar in all the conditions [77].

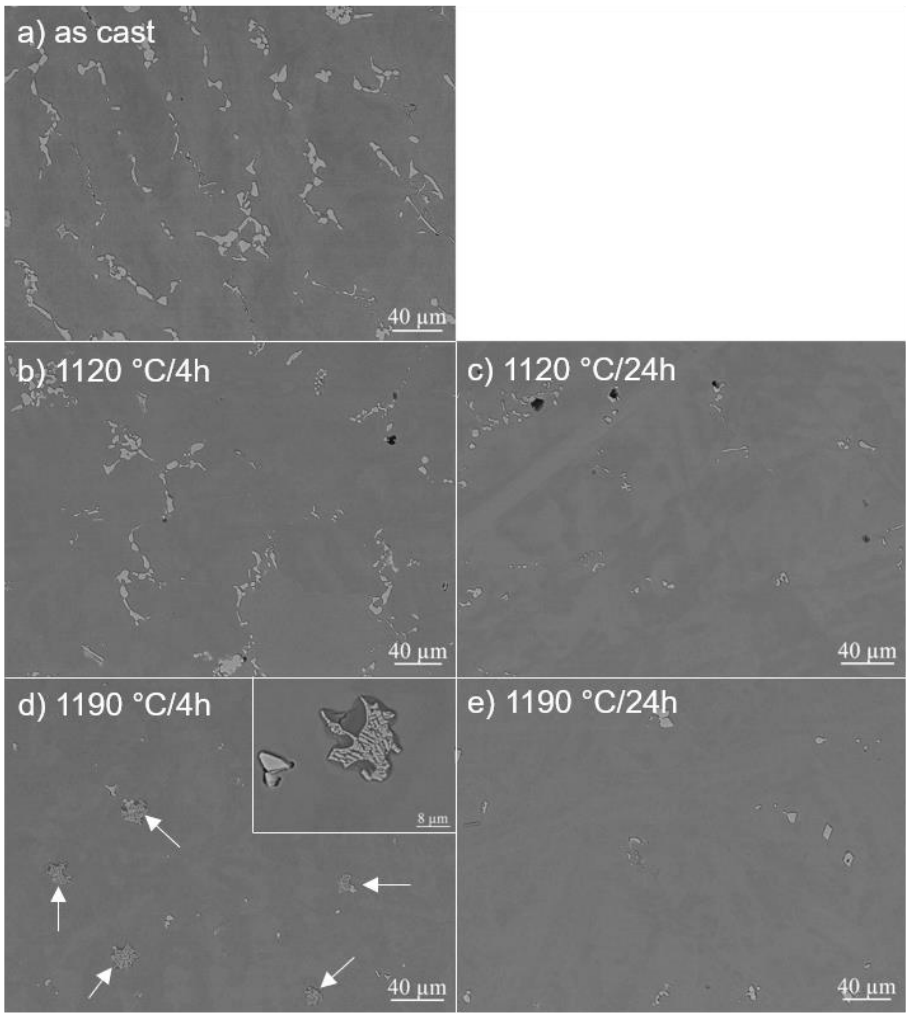

Figure 19. Base metal microstructure for different conditions: a) as-cast; b) 1120 °C/4 h; c) 1120 °C/24 h; d) 1190 °C/4 h with inset showing remelting of the carbide; e) 1190 °C/24 h.

SIMS analysis revealed the presence of minor elements C, S, Si, and B segregated along the grain boundaries and no P was detected. An elemental map for 1190 °C/4 h is shown in Figure 20.

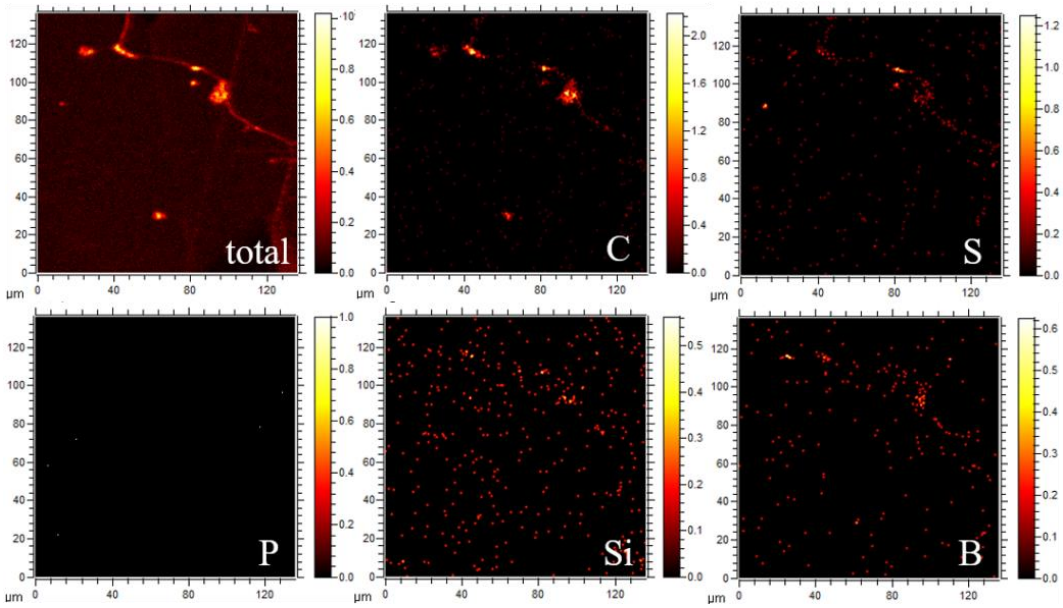

Figure 20. SIMS map showing the segregation of minor elements along the grain boundaries at 1190 °C/4 h.

After the Varestraint testing, no difference was observed in terms of solidification cracking susceptibility. However, regarding the HAZ liquation cracking, the heat treatments at a longer dwell time (i.e., 24 h) at 1120 and 1190 °C exhibited the most extensive cracking, whereas those at 1120, 1160, and 1190 °C with a shorter dwell time of 4 h exhibited the least amount of cracking, as shown in Figure 21. The Avg. TCL for the as-cast condition had an intermediate behavior.

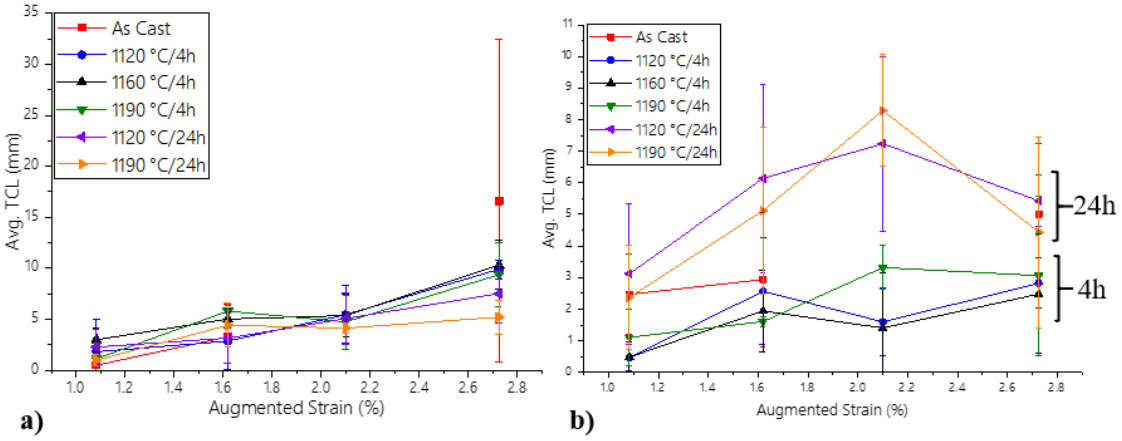

Figure 21. a) Solidification cracking susceptibility and b) HAZ liquation cracking of cast ATI 718Plus.

The on-heating ductility was relatively low with none of conditions exceeding 25% area reduction, as shown in Figure 22. While the ductility after the heat treatments at 1120 °C/4 h and 1190 °C/4 h were comparable within the scatter range, the former reached the NDT at 1140 °C, and the latter reached the NDT at 1120 °C (see Table 9). After 24 h of exposure time, ductility reduced for both the conditions; however it was more severe for the 1190 °C/24 h condition. Both the homogenization heat treatments

reached NDT at 1140 °C. During the on-cooling tests, only the heat treatment at 1190 °C/4 h was able to recover 5% of the ductility with a BTR of 120 °C. All the other conditions failed to recover their ductility.

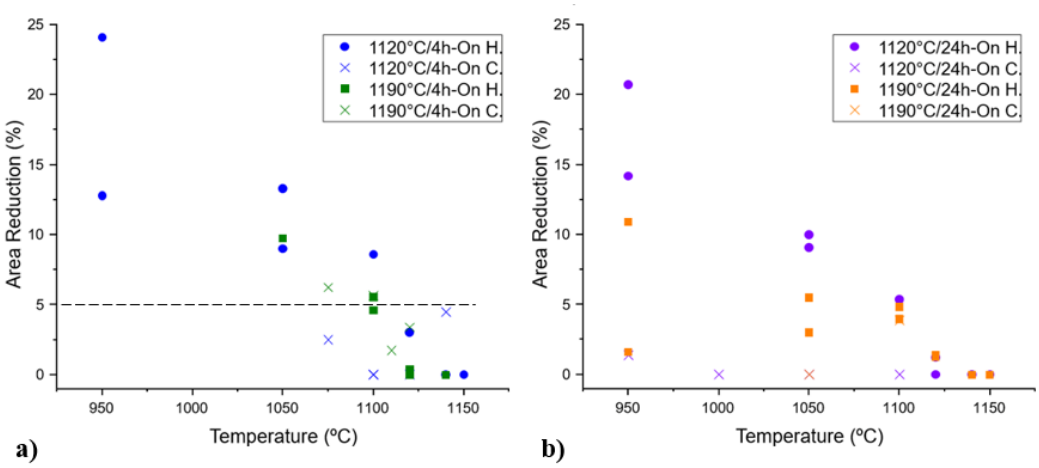

Figure 22. On-heating (On H.) and on-cooling (On C.) signature curves of ATI 718Plus: a) at 4 h; b) at 24 h.

Table 9. Summary of different Gleeble weldability testing parameters; all the temperatures are in °C.

Temperature	Time	NST	NDT	DRT	BTR
1120	4	1225	1140	–	–
	24	1260	1140	–	–
1190	4	1225	1120	1100	120
	24	NA	1140	–	–

The inability to recover the ductility was caused by the extensive melting of the Laves phase and the MC carbides in the inter-dendritic areas for 1120 °C/4 h (see Figure 23 a). However, a constitutional liquation of the MC carbides and an extensive grain boundary melting occurred in the long-dwell heat treatment of 1120 °C/24 h (see Figure 23 b). On the other hand, in the long-dwell heat treatment condition at 1190 °C/24 h (see Figure 23 d), the MC carbides seemed unaffected. However, a grain boundary melting occurred to a higher extent, as compared to 1190 °C/4 h (see Figure 23 c).

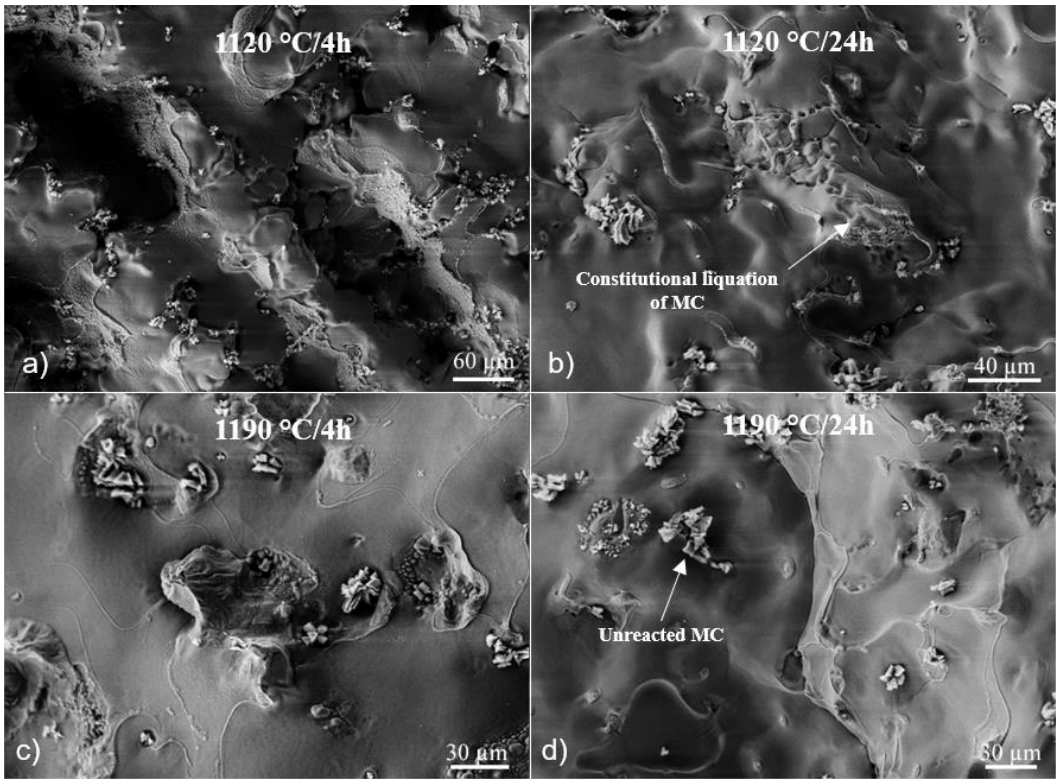

Figure 23. SEM images taken after the on-cooling tests: a) liquation along the inter-dendritic areas in 1120 °C/4 h, pulled to fracture at 1120 °C; b) liquation along the inter-dendritic areas in 1120 °C/24 h, pulled to fracture at 1100 °C; c) constitutional liquation of carbides at the grain boundary in 1190 °C/4 h, pulled to fracture at 1120 °C; d) grain boundary melting in 1190 °C/24 h, pulled to fracture at 1100 °C.

It is possible that the ductility drop was associated with the liquation caused by the solute segregation of S and B, although no evident liquation characteristics were visible below the NDT. These elements were reported to cause liquation at lower temperature than the solidus [50, 52]. Figure 24 shows the effect of Nb as a solute to the solidus temperature. With homogenization heat treatments, the level of Nb changed between the inter-dendritic and dendritic core areas owing to diffusion. It can be seen that with core compositions present at 1120 °C/4 h, the on-cooling peak temperature was well below the solidus, whereas at 1190 °C/4 h, it crossed the solidus line. Comparably, more melting would be expected in the latter case. In case of long-dwell-homogenization heat treatments of 24 h, more Nb was released to the matrix, which shifted the composition towards the right side to the highlighted values, thereby suggesting a more extensive melting.

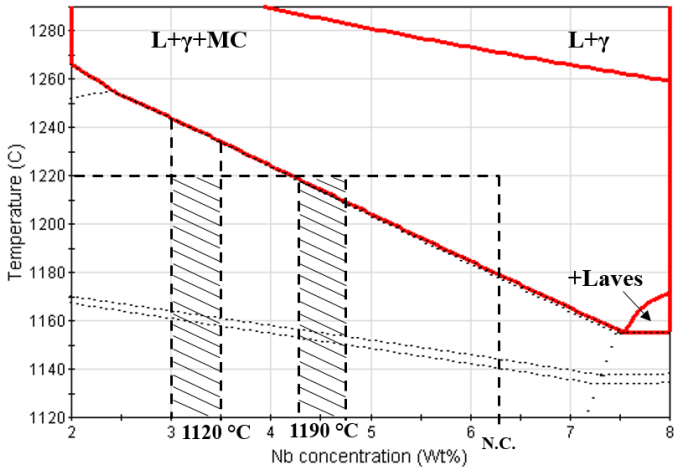

Figure 24. JMatPro isopleth diagram showing the solidus temperature change with a variation in Nb concentration, Ni balance. Nominal composition (N.C.) and compositions in the dendrite cores corresponding to the heat treatments are highlighted with dotted lines corresponding to the intersection with the on-cooling peak temperature.

6.3. Haynes 282 (Paper V)

The base metal microstructure, as obtained through light optical microscopy is shown in Figure 25. The segregation was reduced by increasing the heat treatment temperature both in the matrix and along the grain boundaries. The quantification of the secondary precipitates in terms the of volume fraction (vol.%) showed the highest value of approximately 1.5% in the as-cast condition, and decreased with an increase in the heat treatment temperature to approximately 0.5% after the heat treatment at 1190 °C (see Figure 26). Magnified images of the inter-dendritic region of the 1120 °C/4 h heat treatment condition showed the presence of large MC carbides and small Mo-rich precipitates. At 1160 °C/4 h, Mo-rich precipitates were still present, although to a lesser extent; whereas the treatment at 1190 °C/4 h was able to dissolve them, and only the MC carbides were present.

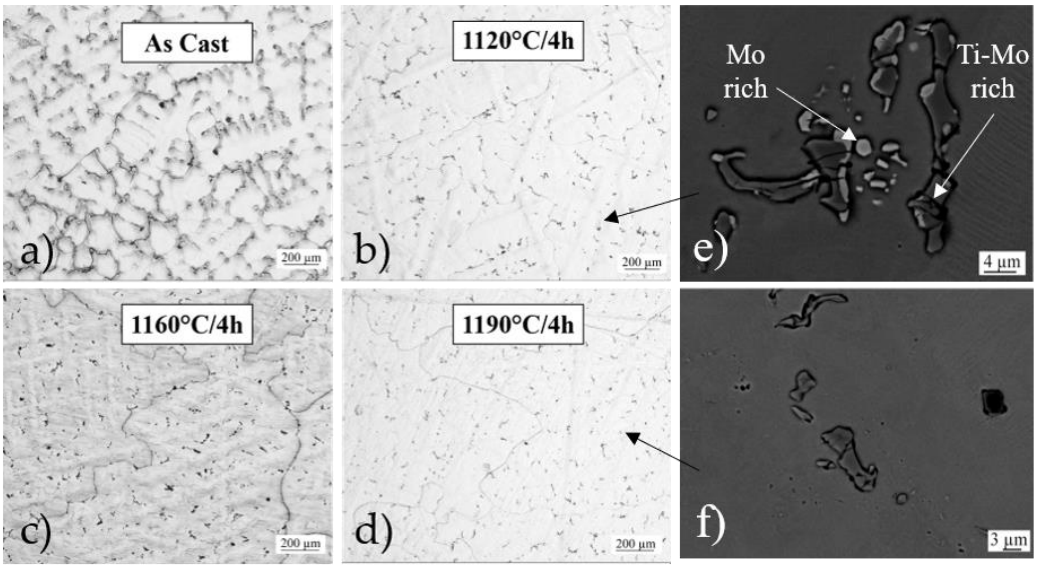

Figure 25. Optical microscopy images showing the extent of segregation in the base metal under different conditions: a) as-cast; b) 1120 °C/4 h; c) 1160 °C/4 h; d) 1190 °C/4 h. SEM images e) and f) showing segregation of Ti–Mo-rich carbides and Mo-rich precipitates in the inter-dendritic areas after the heat treatment at 1120 and 1190 °C/4 h, respectively.

The base metal hardness did not experience any significant change after the heat treatment, with a hardness level in the range of 215–230 HV in the heat-treated conditions, and approximately 245 HV in the as-cast condition (Figure 26). The average grain size of about 1.6 mm remained constant after all the three heat treatments.

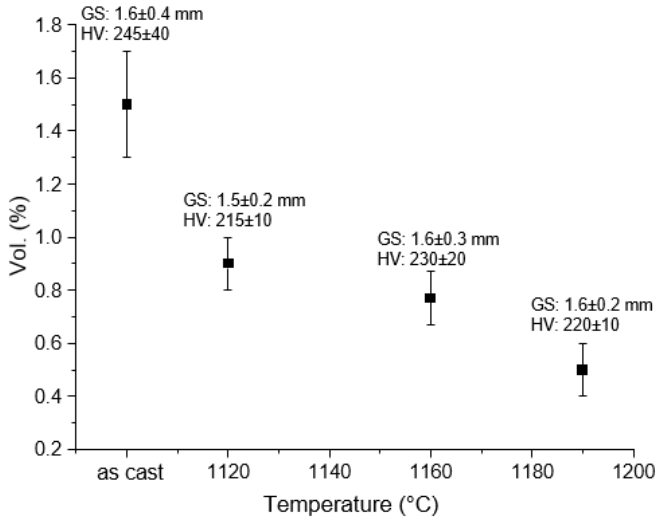

Figure 26. Volume fraction of the precipitates, hardness, and grain size in the as-cast alloy and after pseudo-HIP at 1120, 1160 and 1190 °C of cast Haynes 282.

No effect of homogenization treatments was seen on solidification cracking susceptibility, Figure 27 a). HAZ liquation crack measurements were similar for the pre-weld heat treatments at 1120 and 1160 °C,

which exhibited the least amount of cracking, whereas the 1190 °C heat treatment condition exhibited the highest amount of cracking, Figure 27 b).

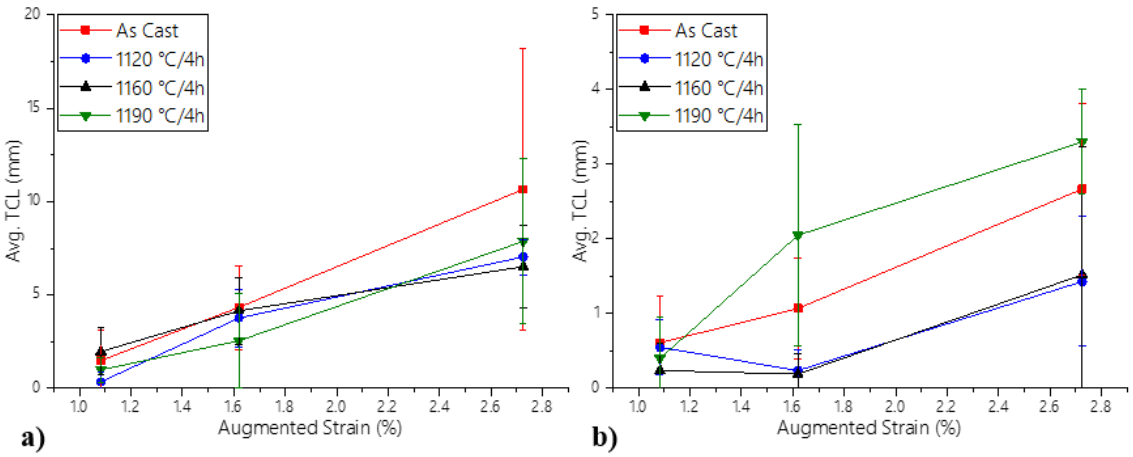

Figure 27. a) Solidification cracking and b) HAZ liquation cracking susceptibility of cast Haynes 282.

Figure 28 shows that the area reduction values for 1120 °C were slightly lower than those of 1190 °C, with a ductility drop starting at approximately 1150 °C, and approaching 0% at 1200 °C. The ductility drop is generally attributed to the formation of a liquid phase responsible for the embrittlement of the grain boundaries.

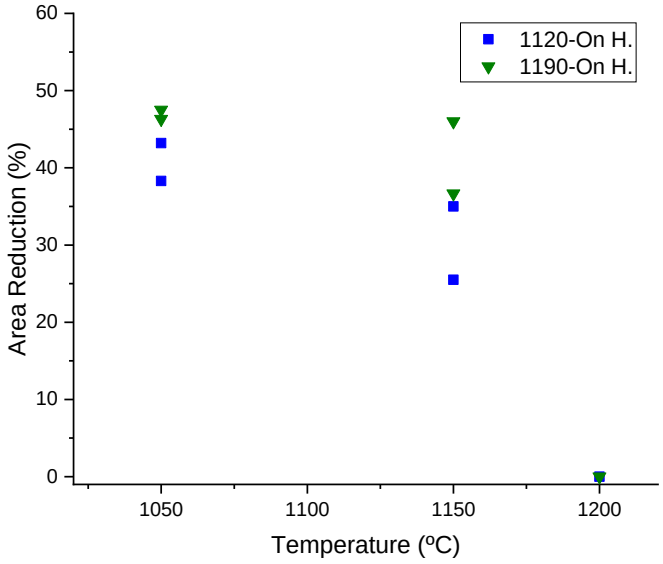

Figure 28. On-heating (On H.) curves for pseudo-HIP conditions at 1120 and 1190 °C/4 h.

Only MC carbides were seen to liquate at 1200 °C in the 1190 °C/4 h heat treatment condition, whereas extensive liquation of MC carbides and secondary phases had occurred at the grain boundaries in the 1120 °C/4 h heat treatment condition (see Figure 29).

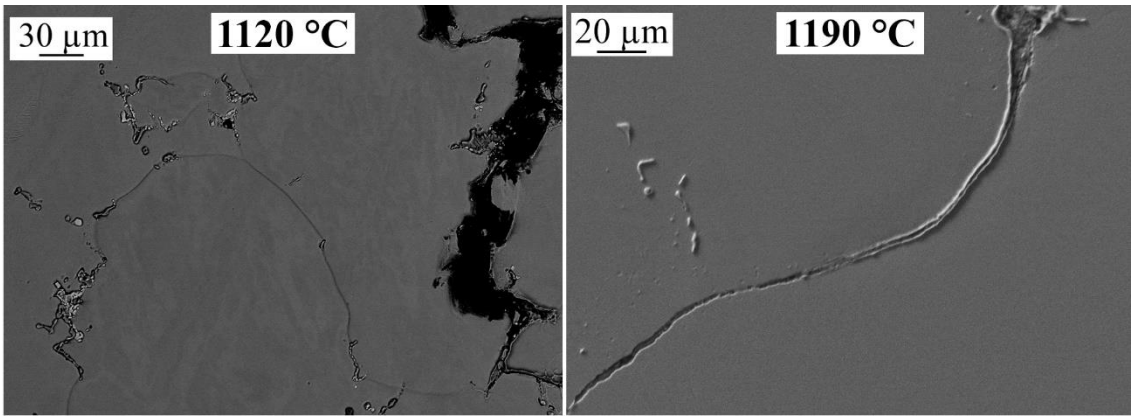

Figure 29. SEM images showing the extent of liquation at a) 1120 °C/4 h and b) 1190 °C/4 h after Gleeble testing at 1200 °C.

At 1190 °C/4 h, B was found to be present in a free form at the grain boundaries (see Figure 30). This temperature was adequately high to dissolve the B-rich particles. The line scans clearly revealed that B was segregated to the grain boundaries. Therefore, the exacerbated cracking in the 1190 °C/4 h condition appeared to be related to the B-segregation from the dissolution of C–B-rich precipitates at the grain boundaries. This phenomenon is known to suppress the local liquation starting temperature, thereby widening the effective melting range of the alloy. The subsolidus melting is not the only effective mechanism for HAZ cracking; in addition to being a significant melting point depressant, B is also a surface active element that improves the wetting property of the liquid so that the liquid is present in a continuous form [21, 25].

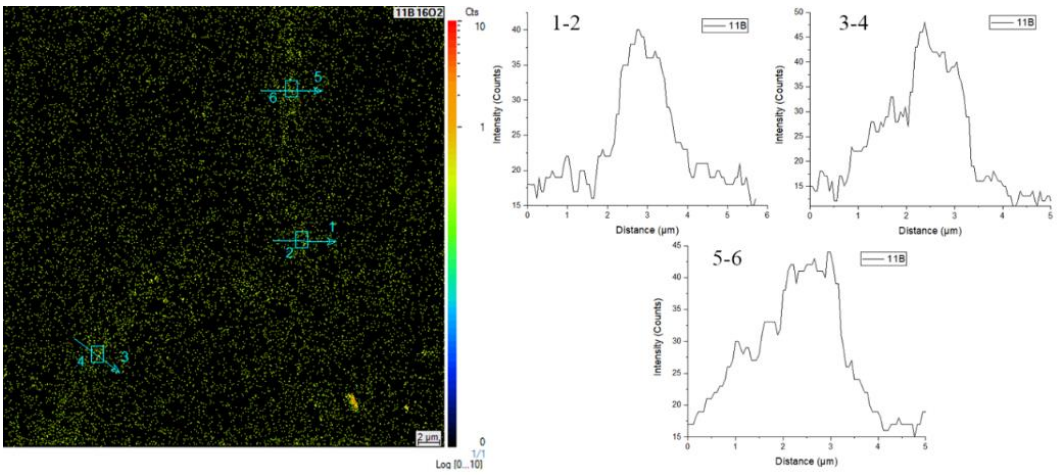

Figure 30. Elemental map (left) and line scans (right) showing B-enrichment along the grain boundaries in the 1190 °C/4 h condition of cast Haynes 282.

6.4. Comparison of Varestraint and hot ductility results

No differences in the solidification cracking susceptibility could be seen from Figure 31. In the as-cast condition, Alloy 718 and Haynes 282 exhibited a similar HAZ liquation cracking susceptibility, whereas ATI 718Plus was more prone to cracking than the former two. However, after the heat treatment at 1120 °C/4 h, the lowest cracking susceptibility was exhibited by Haynes 282, followed by ATI 718Plus and Alloy 718, with the last being the most prone towards HAZ liquation cracking. After being subjected to the heat treatments at 1190 °C/4 h, Alloy 718 was still the most crack-susceptible, with ATI 718Plus and Haynes 282 exhibiting a lesser crack susceptibility (see Figure 31).

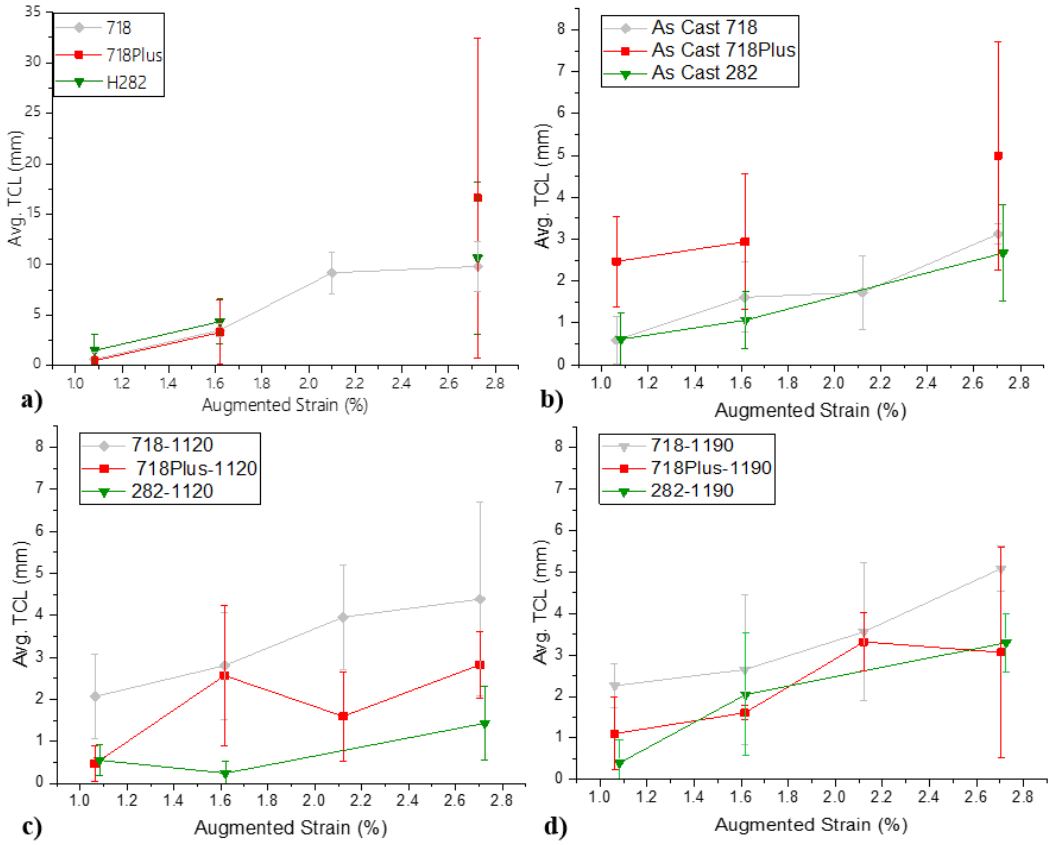

Figure 31. Comparison of a) solidification cracking and b) HAZ liquation cracking susceptibility of as-cast Alloy 718, ATI 718Plus, and Haynes 282. Comparison c) after heat treatment at 1120 °C/4 h and d) 1190 °C/4 h.

Alloy 718 and Haynes 282 had a comparable and relatively high ductility on heating after the heat treatment at 1120 °C/4 h, with steep drops at 1120 and 1190 °C. ATI 718Plus had a lower ductility than the other two, with the ductility drop starting slightly above 1100 °C. The NDT for Haynes 282 could not be measured accurately owing to the unavailability of samples. The NDT values for Alloy 718 and ATI 718Plus were 1150 and 1140 °C, respectively. After heat treatment at 1190 °C/4 h, the on-heating ductility of Haynes 282 remained comparable to that at the lower heat treatment temperature. However, Alloy 718 and ATI 718Plus, in general, exhibited lower ductility values than did Haynes 282, with NDT

values of 1150 and 1120 °C, respectively. As for the on-cooling tests, ATI 718Plus, subjected to heat treatment at 1120 °C/4 h, could not recovery it´s ductility, whereas the DRT for Alloy 718 was at 1130 °C with a BTR of 90 °C. Haynes 282 could recover it´s ductility relatively rapidly at 1150 °C, reaching a similar level as that of the on-heating case. This was followed by Alloy 718 with DRT at 1150 °C and a BTR of 105 °C, ATI 718Plus with DRT at 1100 °C and a BTR of 120 °C (see Figure 32 and Table 10).

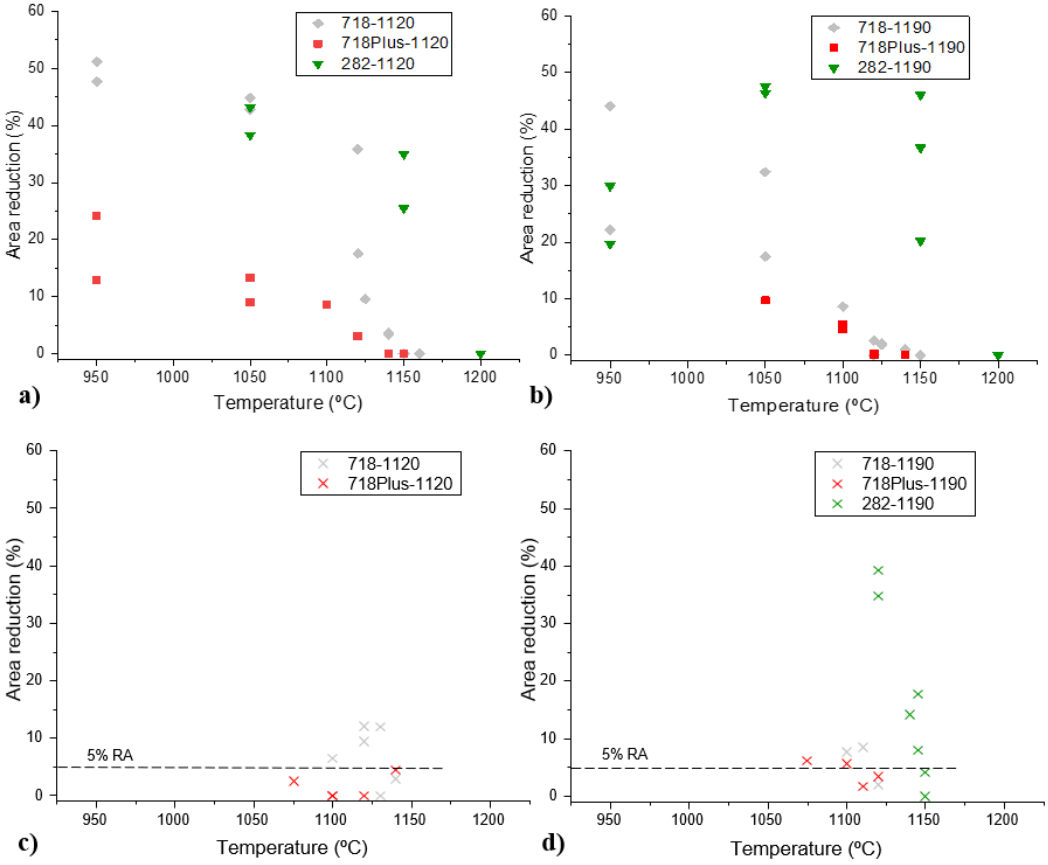

Figure 32. Comparison of on-heating results subjected to heat treatments at a) 1120 °C/4 h and b) 1190 °C/4 h; and on-cooling results subjected to heat treatments of c) 1120 °C/24 h and d) 1190 °C/24 h.

Table 10. Comparison of different Gleeble weldability parameters; all the temperatures are in °C.

	Heat Tr.	NST	NDT	Peak T.	DRT	BTR
Alloy 718	HIP-1120	1270	1150	1220	1130	90
	HIP-1190	1255	1150	1220	1115	105
ATI 718Plus	1120	1225	1140	1220	–	–
	1190	1225	1120	1220	1100	120
Haynes 282	1120	NA	NA	1220	NA	NA
	1190	NA	NA	1220	1150	70

6.5. HAZ liquation cracking mechanisms in cast superalloys

Nb and minor elements affect the cracking susceptibility, as reported in the literature review, as well as the present study. However, two main metallurgical changes related to Nb and non-equilibrium segregation of B can be used to explain the HAZ liquation mechanisms. While the equilibrium segregation decreases with an increase in the heat treatment temperature, the non-equilibrium segregation increases with temperature. Often, during the heat treatments, Nb diffuses from the inter-dendritic areas by the dissolution of Nb-rich Laves phase. The extent of diffusion will increase with an increase in the temperature, along the concentration gradient between the inter-dendritic and dendritic areas and therefore, increases the local Nb level in the dendrite cores (see Figure 33).

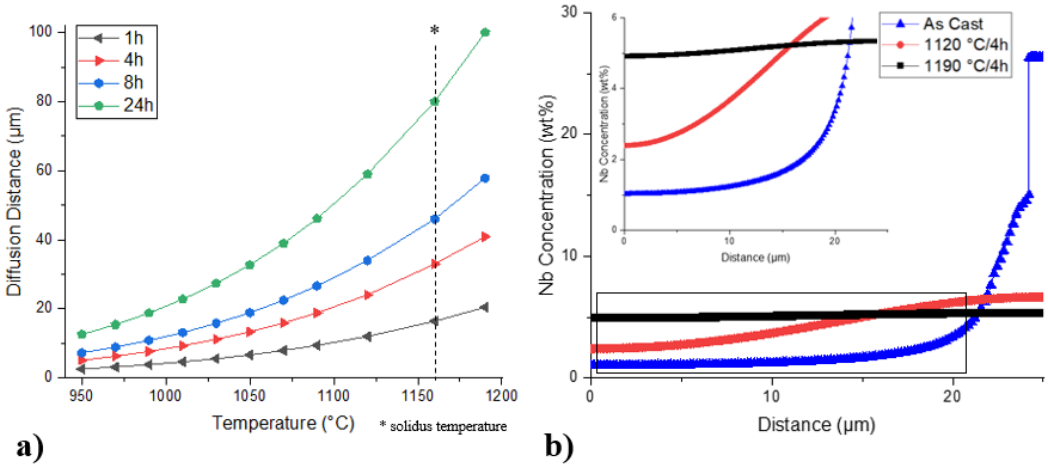

Figure 33. a) Diffusion distances of Nb as function of temperature and exposure time in Alloy 718; b) homogenization effect of Nb after the heat treatments.

These considerations apply for the Nb-bearing Alloy 718 and ATI 718Plus. In Haynes 282, Mo has a similar role as that of Nb in Alloy 718, i.e., as a segregating element. Similar to the previous considerations, Mo diffuses away from the inter-dendritic areas, enriching the level in the dendritic cores, as shown in Figure 34.

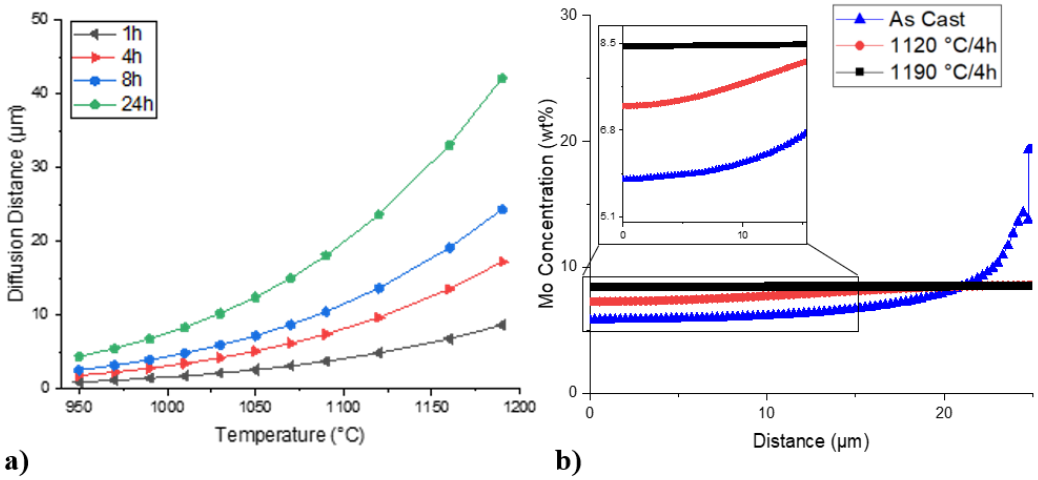

Figure 34. a) Diffusion distances of Mo as function of temperature and exposure time in Haynes 282; b) homogenization effect of Mo after the heat treatments.

To better explain the liquation mechanism in the cast superalloys, the weld heat treatment cycle is divided into three stages as initially proposed by Radhakrishnan et al. [78] for the Nb-bearing superalloy Alloy 718 (see Figure 35). Accordingly, the heating cycle is divided into three stages starting at the eutectic (T_e), followed by the solidus (T_s), and finally, the peak temperature (T_p). Stage 1 is between the ambient temperature and T_e; Stage 2, between T_e and T_s; and Stage 3, between T_s and T_p.

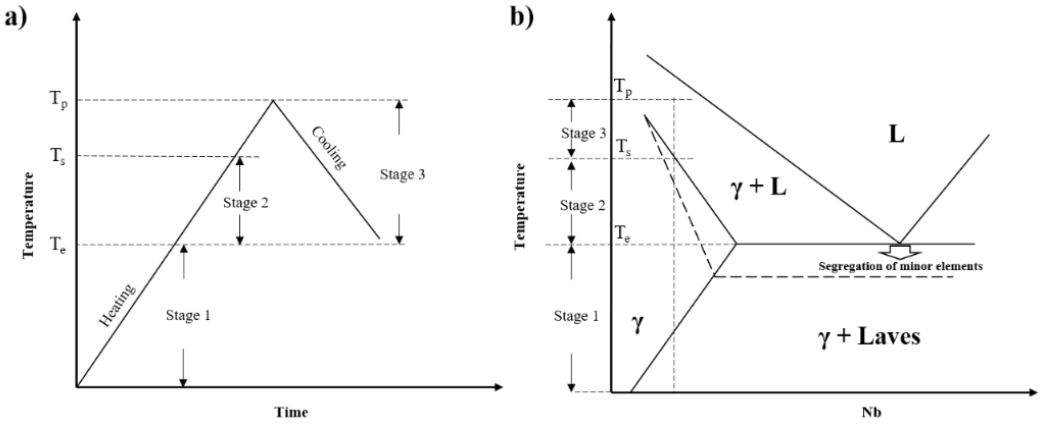

Figure 35. a) HAZ thermal cycle divided into three stages based on the temperature; b) corresponding pseudo-binary phase diagram for Alloy 718; adapted from [78].

Stage 1. Solid-state diffusion and dissolution of secondary precipitates

Stage 1 is characterized by solid-state diffusion and dissolution of precipitates owing to the very rapid heating cycles during the welding. A significant amount of diffusion was expected during this stage up to T_e. The diffusion coefficients of Nb and Mo in Ni were calculated using Arrhenius equation:

$$D = D_0 \times exp\hat{}(Q/RT\,) \qquad \text{Eq. 2}$$

where D is the diffusion coefficient of Nb/Mo in the Ni matrix (m^2/s); D_0 is material constant; Q is the activation energy; R is the gas constant 8.31451 (J/molK); and T is the absolute temperature in Kelvin. The material constant and activation energy values for Nb and Mo are given in Table 11. The diffusion distance l for each temperature was obtained by:

$$l = \sqrt{2Dt} \qquad \text{Eq. 3}$$

where D is the diffusion coefficient obtained by equation (1) and t is the diffusion time (s). The atomic mobility at the grain boundaries is higher than that in the grain interiors and occurs with a lower energy of activation. The l values of Nb and Mo at the grain boundaries were assumed to be the same as in the bulk, as no self-diffusion (D_0) coefficients were found for Nb and Mo at the grain boundaries; however, Q at the grain boundaries was assumed to be half of that in the bulk in fcc metals [79].

Table 11. D_o and Q values for Nb and Mo in Ni [80].

Element	D_0 (m^2/s)	Q (kJ/mol)
Nb	8.8×10^{-5}	257
Mo	1.15×10^{-4}	281

The calculated values of diffusion for Nb and Mo are shown in Figure 36 in the matrix and the grain boundaries. The temperature range used for the Gleeble hot ductility cycles in this study was selected as the temperature range for these calculations as well. Comparatively, a higher diffusivity was obtained for Nb in comparison to Mo. The diffusion distances at a temperature of 1160 °C were estimated to about 0.5 and 0.2 μm for Nb and Mo, respectively in the matrix. A higher diffusivity was obtained along the grain boundaries owing to the lower activation energy required for diffusion. The calculated values were approximately 225 and 125 μm for Nb and Mo, respectively. With such a high diffusion rate, significant dissolution is expected to occur along the grain boundaries.

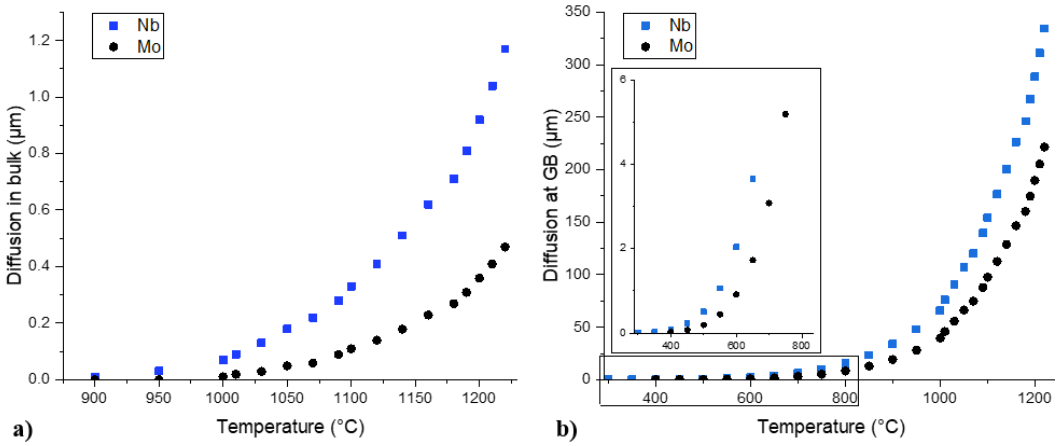

Figure 36. Plots showing diffusion distances for Nb and Mo in Ni/Haynes 282: a) in the bulk of the material; b) at the grain boundary.

Although, no melting is expected in this stage, as the temperatures are below the minimum solidus temperature, it can still occur owing the solute segregation, especially along the grain boundaries. Small impurity elements, such as S, P, and B preferentially tend to segregate along the grain boundaries, to suppress the local melting temperature during the heating cycle [20, 49, 52]. During the cooling cycle, they help in extending the solidification range below the minimum solidus of the alloy.

Stage 2. Liquation of precipitates

Melting of Laves occurs as the weld thermal cycle temperature reaches T_e. The extent of melting is dependent on the volume fraction of Laves in the material. A higher contribution is expected in the as-cast condition. Figure 37 shows an image of a HAZ liquation cracking via Laves liquation in Alloy 718. After the homogenization heat treatments, the volume fraction of Laves decreased with increasing homogenization temperature and the contribution to the liquation through Laves, therefore, decreased. Another mechanism for liquation in this stage was through the constitutional liquation of carbides.

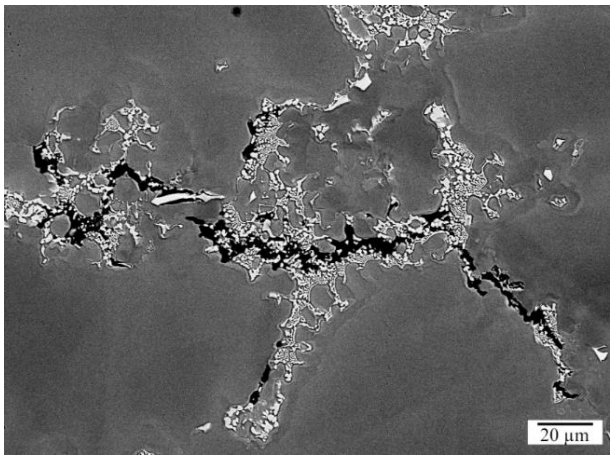

Figure 37. Liquation of Laves in as-cast Alloy 718.

Stage 3. Supersolidus liquation

The areas next to the FZ, e.g., the partially melted zone, undergo matrix melting as the temperatures reach above the solidus temperature. The extent of melting depends on the local solute content. This also applies to the grain boundaries, where the solute segregation (Nb) can reduce the melting point. As discussed in the previous section, the solute segregation along the grain boundaries lowers the liquation temperature along the grain boundaries. At higher temperatures, the extent of Nb along the grain boundaries and in the matrix governs the liquation extent in the Nb-bearing superalloys. In Figure 38 an example is shown for Alloy 718, ATI 718Plus, and Haynes 282. The compositions highlighted represent the matrix core compositions after the HIP and pseudo-HIP treatments. If the alloys were exposed to heating cycles with a maximum temperature of 1220 °C, the material subjected to a heat treatment at 1190 °C/4 h would undergo more extensive melting as compared to that subjected to a heat treatment at 1120 °C/4 h in the case of cast superalloys 718 and ATI 718Plus. Similarly, in the case of cast Haynes 282, an isopleth as a function of varying amounts of Mo showed a solidus temperature above 1250 °C; therefore, no subsolidus melting was expected at 1220 °C.

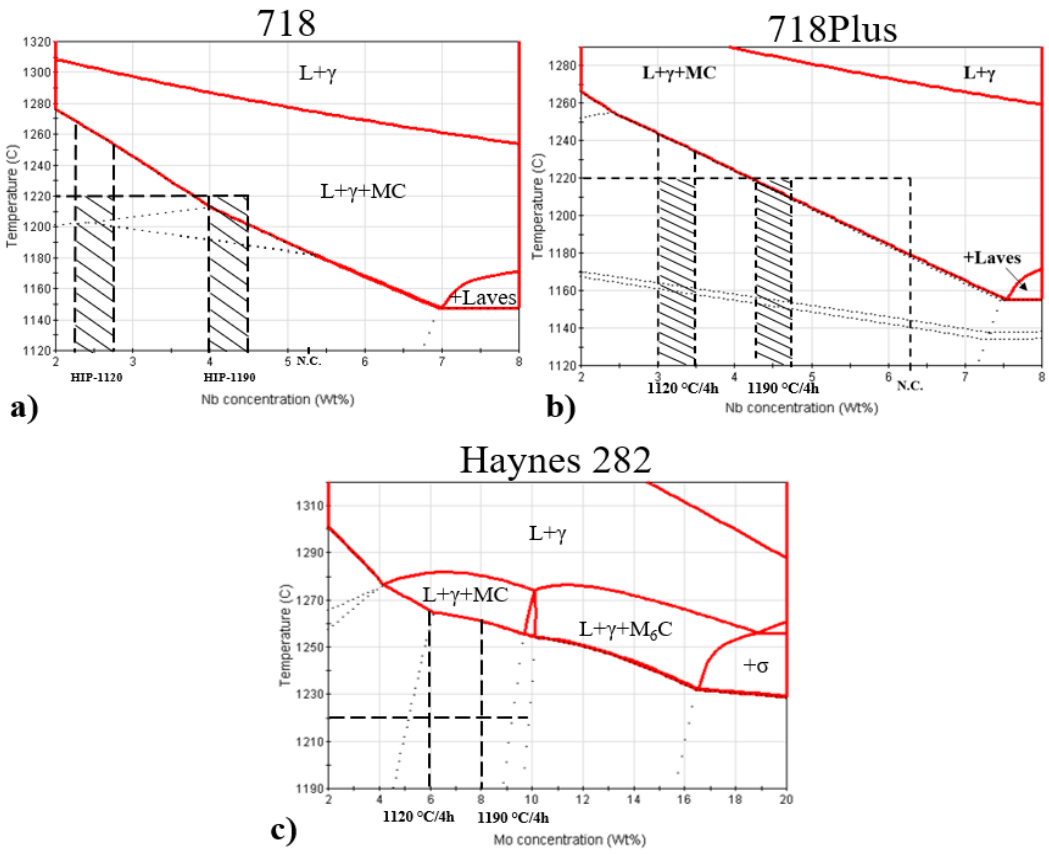

Figure 38. JMatPro isopleth diagrams showing the solidus temperature as a function of Nb concentration for a) Alloy 718 and b) ATI 718Plus, and c) as a function of Mo concentration for Haynes 282. Compositions corresponding to the heat treatments are highlighted with dashed lines corresponding to the intersection with the on-cooling peak temperature.

7. Conclusions

The weldability of precipitation hardening cast Ni-based superalloys were investigated by Varestraint and Gleeble tests. The conclusions regarding the research questions raised at the beginning of this thesis are as follows:

RQ 1: How do the microstructural changes after the homogenization heat treatments affect HAZ liquation cracking susceptibility of cast superalloys – Alloy 718, ATI 718Plus, and Haynes 282?

Cast Alloy 718

- HIP-1120 conducted at 1120 °C/4 h was able to partially dissolve the Laves phase. This HIP treatment exhibited a high on-heating and rapid on-cooling ductility recovery. The liquation was contributed by the melting of the Laves phase, constitutional liquation of MC carbides, and solute segregation along the grain boundaries.
- HIP-1190 conducted at 1190 °C/4 h resulted in a more homogenized microstructure and a total dissolution of the Laves phase. The higher heat treatment temperature also resulted in a larger grain size in comparison to that with HIP-1120. The homogenization of Nb lowered the temperature required for the initiation of the supersolidus melting along the grain boundaries, together with contribution from the solute segregation of minor elements. The extensive melting along the grain boundaries and the larger grain size led to an overall lower on-heating ductility and delayed recovery on cooling, which caused a higher HAZ liquation cracking.

Cast ATI 718 Plus

- The HAZ liquation cracking susceptibility was found to be related to the heat treatment dwell time, rather than the soak temperature. The heat treatments at 1120 and 1190 °C of 24 h dwell time resulted in a more extensive cracking than with 1120, 1160, and 1190 °C/4 h dwell time.
- Heat treatments at 1120 and 1190 °C/4 h exhibited similar on-heating ductility. The latter had the lowest NDT at 1120 °C, with the constitutional liquation of the MC carbides starting at approximately 1140 °C. The condition of 1190 °C/4 h was the only one to recover its ductility on cooling at 1100 °C, resulting in a BTR of 120 °C. The liquation was mainly caused by a melting of the partially dissolved Laves in the material heat-treated at 1120 °C/4 h. The heat treatment at 1190 °C/4 h exhibited extensive constitutional liquation and partial grain boundary melting. However, the HAZ liquation cracking susceptibility was comparable.

- The long-dwell heat treatment at 1190 °C/24 h exhibited the lowest overall ductility. The homogenization heat treatments at both 1120 °C/24 h and 1190 °C/24 h reached the NDT at 1140 °C, but failed to recover in the on-cooling tests owing to the extensive Laves liquation in the former and supersolidus melting in the later, which also caused more severe HAZ cracking than in the 4 h dwell heat treatments.

Cast Haynes 282

- Material conditions subjected to homogenization heat treatments at 1120 and 1160 °C/4 h exhibited comparable HAZ liquation cracking. The heat treatment at 1190 °C/4 h was the most crack-susceptible condition. The B-rich precipitates, possibly carboborides, were found in the conditions of 1120 and 1160 °C/4 h, whereas the heat treatment at 1190 °C/4 h completely dissolved the carboborides, which led to B atoms being released from the dissolution of these precipitates, and segregated to the grain boundaries;
- The complete dissolution of C–B particles and the segregation of B at the grain boundaries at 1190 °C exacerbated the HAZ cracking.

RQ 2: What are the mechanisms in HAZ liquation cracking during the welding of these cast superalloys?

- Liquation from solute segregation, which is effective at lower temperatures: It was found that B had a very important role as minor element segregating along the grain boundaries.
- Precipitate liquation through the liquation of Laves phase in Nb-bearing superalloys, i.e., Alloy 718 and ATI 718Plus, and the constitutional liquation of the carbides.
- Supersolidus melting, whose extent depends on the local solute content in the matrix and along the grain boundaries.

Each of the above-mentioned mechanisms contributed to the overall extent of liquation, which in turn also affected the HAZ liquation cracking susceptibility. It is clear that the HIP/pseudo-HIP treatments, which minimized the overall extent of liquation, also minimized the extent of HAZ liquation cracking. From the present investigation, it may be inferred that the HIP-1120 °C at 4 h for Alloy 718, pseudo-HIP 1120 °C at 4 h for ATI 718Plus, and pseudo-HIP at 1120 and 1160 °C at 4 h for Haynes 282 were beneficial. Therefore, a common homogenization heat treatment at 1120 °C and an exposure time of 4 h is recommended for the three cast superalloys.

8. Future work

The mechanical properties of the welded parts after HIP/Pseudo-HIP should be investigated. In the present study, the effect of homogenization heat treatments was investigated with regard to weld-cracking susceptibility; however, it is also important to know how it affects the material performance. This also needs to be considered in the context of requirements for specific applications. For example, cast Alloy 718 components subjected to creep strength will require a larger grain size, which could be achieved by HIP treatment at 1190 °C. However, this material condition exhibited more extensive HAZ liquation cracking than the HIP at 1120 °C condition.

Cast superalloys ATI 718Plus and Haynes 282 were subjected to water quenching post pseudo-HIP treatments to avoid precipitation hardening of phases. This is, however, not possible in an industrial scenario owing to the large component sizes and issues related to distortions. Therefore, a slower cooling, which minimizes the hardening of the material and non-equilibrium segregation of B is recommended, as they are critical factors for hot cracking formation.

A more detailed grain boundary analysis using transmission electron microscopy/atom probe tomography (TEM/APT) is suggested to investigate the chemical composition variation after the diffusion. In-situ SEM tests at high temperatures are recommended to study the grain boundary embrittlement effect due to solute segregation.

Furthermore, the role of Nb and Mo at different compositions need to be experimentally verified, e.g., via DSC measurements.

9. Acknowledgments

First and foremost, I would like to thank my supervisor, Assoc. Professor Joel Andersson for providing me the opportunity to work on such an interesting research project. I thank him for believing in me and supporting me throughout this journey, especially by providing me an invaluable freedom, which allowed me to grow in different aspects.

I am sincerely grateful to Professor Olanrewaju Ojo from University of Manitoba (Canada) for all the intense, but inspiring discussions on the topic of hot cracking, and always providing me with new insights. I also want to thank Professor Boian Alexandrov from Ohio State University (USA) for providing inputs to my research work, and Emeritus Professor Hasse Fredriksson from KTH for the valuable feedback given to me during my Licentiate seminar.

At the Department of Industrial and Materials Science at Chalmers University of Technology, I would like to thank my examiner Professor Lars Nyborg and group leader Professor Uta Klement for their support. Thanks are also due to Yiming Yao for exhibiting enormous patience with me at the SEM. I also thank Swathi, Mahesh, and Bala for sharing the office space with me. I also wish to thank my numerous fellow PhD students at Chalmers for the fun time I spent during the laboratory sessions.

I am grateful for the opportunity given to me to work with the Welding Group at the Department of Engineering Science at University West. I would like to thank Kjell Hurtig for the help provided with the Varestraint and Gleeble equipment. My thanks also go to Kenneth Andersson for the good training provided to me with metallographic preparation and SEM. I wish to express my thanks to other friends and colleagues there for the pleasant working environment.

I am very grateful for the support received from GKN Aerospace Sweden AB. I would like to thank Géraldine Puyoo and Ceena Joseph for the support provided during the project.

Next, many thanks to the International Institute of Welding (IIW) for providing a platform for me to share my work, and to the members for the engaging discussions that I had with them. Special thanks go to Elin Westlin and Asun Valiente at commission IX-H for creating a supportive environment for young professionals.

At the Department of Chemistry at Chalmers University of Technology, I thank Per Malmberg for helping me with ToF-SIMS, and Aurelién Thomen at Gothenburg University for the nanoSIMS analysis.

I had a great opportunity to work with William Fransson, Mathieu Lafarie, and Lujain Banbouk during their internships. I wish you all the best of luck with your future! I also appreciated working with many Bachelor and Master students at Chalmers and University West. It was a lot of fun, and I learned a lot from you.

My sincere appreciation goes to Fabian, with whom I shared my PhD journey and also for being a companion in many of my adventures. Furthermore, I will never forget our road trips in Australia and US! My thanks to Swathi, for the numerous discussions we had on spirituality and on food, which I also had the opportunity to "taste", and to Seshendra for surprising me by "calculating" my horoscope over a meal. Thank you, Xiaoxiao (Master) for sharing your experience on fine arts; and Andreas, for allowing me to experience the "real" Swedish culture and helping me out with the renovation work. Nages and Wellington, you have taken the parties to a new level and perhaps it is time for me to stepdown; Suhas, thank you for bearing with my "bad" humor; Tahira, thank you for feeding me multiple times over the years even though you did not have much free time (I like your biryani a lot!).

I have had the pleasure of coming across many other people during these years. My sincere gratitude to Shifu QiXia for hosting me at the Fawang Temple, together with the little Kung Fu fighters; Master Ali for training me on how to ride on a horseback like a "warrior"; my fellow "Sidakers" for sharing your experiences and teaching me about Sikhi, and the night walks under an ocean of stars, with the bears scaring us out in the blueberry farm!; Inni for our deep conversations and your inspiring poetry; Neelu aunty for hosting me in Surrey; Luca for organizing dinners back in Italy; and my cousin, Gurwinder, in Punjab for teaching me what it means to be a farmer.

Last but not the least, this amazing journey would not have been possible without the support of my parents. Thank you, my father Sardar Harbhajan Singh and my mother Sardarni Paramjit Kaur, for your unconditional love. My thanks also to my lovely sisters, Maninder and Amandeep; maybe, one day we will all be united. My nephew Loveneet, you have been an inspiration to me ever since you were born. Gurmehak and little Sukhman, I wish we would play more often in future.

10. References

[1] H.L. Eiselstein, Age-hardenable nickel alloy, Patent no. 3,046,108, 1962.

[2] O.W. Ballou, M.W. Coffey, History of Cast Inco 718. Superalloys 1988, 1988, 469-473.

[3] W. D. Cao, R. Kennedy, Role of chemistry in 718-type alloys–Allvac® 718Plus™ alloy development, in Superalloys 2004, 2004, 91–99.

[4] L. M. Pike, Development of a fabricable gamma-prime (γ′) strengthened superalloy, in Superalloy 2008, 2008, 191–200.

[5] B. Peterson, D. Frias, D. Brayshaw, R. Helmink, S. Oppenheimer, E. Ott, R. Benn, M. Uchic, On the Development of Cast ATI 718Plus® Alloy for Structural Gas Turbine Engine Components, 2012.

[6] J. Andersson, Weldability of precipitation hardening superalloys–influence of microstructure. Phd Thesis, Chalmers University of Technology, 2011.

[7] R. G. Thompson, Microfissuring of alloy 718 in the weld heat-affected zone, JOM, 1988 40(7), 44–48.

[8] W. A. Baeslack and D. E. Nelson, Morphology of weld heat-affected zone liquation in cast alloy 718, Metallography, 1986, 19(3), 371–379.

[9] M.L. Barron, Crack Growth-Based Predictive Methodology for the Maintenance of the Structural Integrity of Repaired and Nonrepaired Aging Engine Stationary Components, GE Aircraft Engines Cincinnati OH, 1999.

[10] S. M. Snyder, E. E. Brown, Laves free cast + hip nickel base superalloy. U.S. Patent No 4,750,944, 1988.

[11] D. F. Paulonis, J. J. Schirra, Alloy 718 at Pratt & Whitney–Historical perspective and future challenges, Superalloys, 2001, 718(625,706), 13-23.

[12] C.T. Sims, N.S. Stoloff, W.C. Hagel, Superalloys II, Wiley-Interscience, 1987.

[13] M. J. Donachie, S. J. Donachie, Superalloys: a technical guide, ASM International, 2002.

[14] J.F. Radavich, The physical metallurgy of cast and wrought alloy 718, Superalloy 718-Metallurgy and Applications, 1989. 229-240.

[15] A. Mitchell, A. J. Schmalz, C. Schvezov, S. L. Cockroft, The Precipitation of Primary Carbides in Alloy 718, 1994, pp. 65–78.

[16] S. Singh, Varestraint Weldability Testing of Cast Superalloys, Licentiate Thesis, Chalmers University of Technology, 2018.

[17] W. D. Cao, Solidification and solid state phase transformation of Allvac® 718Plus™ alloy, in Superalloys 718, 625 and Various Derivatives 2005, 2005, 66–177.

[18] J. Andersson, G. Sjöberg, J. Larsson, Investigation of Homogenization and its Influence on the Repair Welding of Cast Allvac 718Plus, in Proceedings of The 7th International Symposium on Superalloy 718 and Derivatives, TMS (The Minerals, Metals and Materials Society), 2010, 439–454.

[19] J. Caron, Weldability and Welding Metallurgy of Haynes 282 Alloy, In Proceedings of the 8th International Symposium on Superalloy 718 and Derivatives, John Wiley & Sons, 2014, 273–286.

[20] L. O. Osoba, R. G. Ding, O. A. Ojo, Improved Resistance to Laser Weld Heat-Affected Zone Microfissuring in a Newly Developed Superalloy HAYNES 282, Metallurgical and Materials Transactions A, 2012, 43(11), 4281–4295.

[21] H. Matysiak, M. Zagorska, J. Andersson, A. Balkowiec, R. Cygan, M. Rasinski, M. Pisarek, M. Andrzejczuk, K. Kubiak, K.J. Kurzydlowski, Microstructure of Haynes® 282® Superalloy after Vacuum Induction Melting and Investment Casting of Thin-Walled Components, Materials, 2013, 6(11), 5016–5037.

[22] Haynes® 282® alloy. Haynes International, 2018.

[23] W.I. Pumphrey, P.H. Jennings, A consideration of the nature of brittleness at temperatures above the solidus in castings and welds in aluminium alloys, Journal of the Institute of Metals, 1948, 75(4), 235-256.
[24] W.S. Pellini, Strain theory of hot tearing, Foundry, 1952, 80(11),125–133.
[25] J. Borland, Generalized theory of super-solidus cracking in welds (and castings), British Welding Journal 1960, 7(8), 508–512.
[26] F. Matsuda, H. Nakagawa, K. Sorada, Dynamic Observation of Solidification and Solidification Cracking during Welding with Optical Microscope (I): Solidification Front and Behavior of Cracking , Materials, Metallurgy & Weldability, Transactions of JWRI, 1982, 11(2), 67–77.
[27] S. Kou, Welding metallurgy, 2nd ed. Hoboken, N.J: Wiley-Interscience, 2003.
[28] J.N. Dupont, J.C. Lippold, S.D. Kiser, Welding metallurgy and weldability of nickel-base alloys, Hoboken, N.J: John Wiley & Sons, 2009.
[29] J.N. DuPont, C.V. Robino, A.R. Marder, Solidification and weldability of Nb-bearing superalloys, Welding Research Supplement, 1998, 417-431.
[30] L.O. Osoba, A study on laser weldability improvement of newly developed Haynes 282 superalloy, Phd Thesis, University of Manitoba, 2012.
[31] M.J. Cieslak, T.J. Headley, R.B. Frank, The welding metallurgy of custom age 625 PLUS alloy, Welding Journal, 1989, 68(12), 473-482.
[32] K. Shinozaki, P. Wen, M. Yamamoto, K. Kadoi, Y. Kohno, T. Komori, Effect of grain size on solidification cracking susceptibility of type 347 stainless steel during laser welding, Quarterly Journal of the Japan Welding Society, 2010, 29(3), 90s-94s.
[33] S. Singh, J. Andersson, Varestraint weldability testing of cast ATI® 718 Plus™ – A comparison to cast Alloy 718, Welding in the World, Volume 63, 389–399.
[34] L. Karlsson, H. Nordén, H. Odelius, Overview no. 63 Non-equilibrium grain boundary segregation of boron in austenitic stainless steel—I. Large scale segregation behaviour, Acta Metallurgica, 1988, 36(1), 1–12.
[35] L. Karlsson, H. Norden, Grain boundary segregation of boron, An experimental and theoretical study, Le Journal de Physique Colloques, 1986, 47(C7), C7-257.
[36] L. Karlsson and H. Nordén, Overview no. 63 Non-equilibrium grain boundary segregation of boron in austenitic stainless steel-II, Fine scale segregation behaviour, Acta Metallurgica, 1988, 36(1), 13–24.
[37] J.C. Lippold, Welding metallurgy and weldability. Hoboken, New Jersey: John Wiley & Sons Inc, 2015.
[38] J.J. Pepe, W.F. Savage, Effects of constitutional liquation in 18-Ni maraging steel weldments (Microsegregation and grain boundary liquation in heat affected zone of 18-Ni maraging steel welds), Welding Journal, Research Supplement, 1967, vol. 46.
[39] S. Singh, F. Hanning, J. Andersson, Influence of hot isostatic pressing on hot ductility of cast Alloy 718: effect of Niobium and minor elements on liquation mechanisms, Metallurgical and Materials Transactions A, 2020, DOI: 10.1007/s11661-020-06004-8.
[40] S. Singh, F. Hanning, J. Andersson, Influence of homogenisation treatments on the hot ductility of Cast ATI® 718Plus®: Effect of Niobium and minor elements on liquation characteristics, Materials Science and Engineering A, 2021, Volume 799, 140151.
[41] S. Singh, J. Andersson, Heat-Affected-Zone Liquation Cracking in Welded Cast Haynes® 282®, 2020, vol. 10, p. 11.
[42] B. Weiss, G. E. Grotke, Physical Metallurgy of Hot Ductility Testing, Welding Research Supplement, 1972, 471–487.
[43] M. C. Chaturvedi, Liquation Cracking in Heat Affected Zone in Ni Superalloy Welds, Materials Science Forum, 2007, vol. 546–549, 1163–1170.

[44] S.L. West, W.A. Baeslack, T.J. Kelly, Morphology of weld heat-affected zone liquation cracking in Ta-modified cast Alloy 718, Metallography, 1989, 23(3), 219-229.
[45] I. Woo, K. Nishimoto, K. Tanaka, M. Shirai, Effect of homogenisation heat treatment on heat affected zone cracking susceptibility. Study of weldability of Inconel 718 cast alloy (3rd Report), Welding International, 2000, 14(7), 523–532.
[46] S. Benhaddad, N.L. Richards, U. Prasad, H. Guo, M.C. Chaturvedi, The Influence of B, P and C on Heat-Affected Zone Micro-Fissuring in Inconel Type Superalloy, in Superalloys 2000 (Ninth International Symposium), 2000, 703–711.
[47] X. Huang, M.C. Chaturvedi, N.L. Richards, J.Jackman, The effect of grain boundary segregation of boron in cast alloy 718 on HAZ microfissuring—A SIMS analysis, Acta Materialia, 1997, 45(8), 3095–3107.
[48] T. Alam, P.J. Felfer, M. Chaturvedi, L.T. Stephenson, M.R. Kilburn, J.M. Cairney, Segregation of B, P, and C in the Ni-Based Superalloy, Inconel 718, Metallurgical and Materials Transactions, 2012, 43(7), 2183–2191.
[49] X. Huang, M.C. Chaturvedi, N.L. Richards, J. Jackman, The effect of grain boundary segregation of boron in cast alloy 718 on HAZ microfissuring-A SIMS analysis, Acta Materialia, 1997, 45(8), 3095–3107.
[50] Y. Zhu, S. Zhang, T. Zhang, L. Lou, Y. Tong, X. Ning, Z. Hu, X. Xie, Effect of P, S, B and Si on the Solidification Segregation of Inconel 718 Alloy, in Superalloys 718, 625, 706 and Various Derivatives (1994), 1994, 89–98.
[51] K. Vishwakarma, M. Chaturvedi, A Study of HAZ Microfissuring in a Newly Developed Allvac 718 Plus Superalloy, in Superalloy 2008, 2008, 241–250.
[52] K.R. Vishwakarma, M.C. Chaturvedi, Effect of boron and phosphorus on HAZ microfissuring of Allvac 718 Plus superalloy, Materials Science and Technology, 2009, 25(3), 351–360.
[53] J. Jacobsson, J. Andersson, A. Brederholm, H. Hanninen, Weldability of Ni-Based Superalloys Waspaloy® and Haynes® 282® - A Study Performed with Varestraint Testing, Research & Reviews: Journal of Material Sciences, 2016, 4(4).
[54] F. Hanning and J. Andersson, Weldability of wrought Haynes® 282® repair welded using manual gas tungsten arc welding, Welding in the World, 2018, 62(1), 39–45.
[55] R. G. Thompson, J. J. Cassimus, D. E. Mayo, J. R. Dobbs, The relationship between grain size and microfissuring in alloy 718, Welding Journal, 1985, 64(4), 91-96.
[56] I. Woo, K. Nishimoto, K. Tanaka, M. Shirai, Effect of grain size on heat affected zone cracking susceptibility, Study of weldability of Inconel 718 cast alloy (2nd Report), Welding International, 2000, 14(7), 514–522.
[57] J. Jacobsson, J. Andersson, Weldability of Superalloy Alloy 718 and ATI® 718Plus™ - A study performed with Varestraint Testing, Materials Testing, 2017, 59(9), 769–773.
[58] X. Huang, N.L. Richards, M.C. Chaturvedi, Effect of Grain Size on the Weldability of Cast Alloy 718, Materials and Manufacturing Processes, 2004, 19(2), 285–311.
[59] T. Kannengiesser, T. Boellinghaus, Hot cracking tests—an overview of present technologies and applications, Welding in the World, 2014, 58(3), 397–421.
[60] W.F. Savage, C.D. Lundin, The Varestraint test, Welding Journal, 1965, 44(10), 433s-442s.
[61] S. Singh, W. Fransson, J. Andersson, A. Brederholm, H. Hänninen, Varestraint Weldability Testing of ATI 718Plus®—Influence of Eta Phase, in Proceedings of the 9th International Symposium on Superalloy 718 & Derivatives: Energy, Aerospace, and Industrial Applications, Cham: Springer International Publishing, 2018, 929–937.

[62] S. Singh, K. Hurtig, J. Andersson, Investigation on effect of welding parameters on solidification cracking of austenitic stainless steel 314, Procedia Manufacturing, 2018, vol. 25, 351–357.
[63] K. Kadoi, S. Ueda, S. Tokita, H. Inoue, Effect of MC carbide formation on weld solidification cracking susceptibility of austenitic stainless steel, Journal of Alloys and Compounds, 2020, vol. 828, 154423.
[64] C.C. Chang, C.L. Chen, J.Y. Wen, C.M. Cheng, C.P. Chou, Characterization of Hot Cracking Due to Welding of High-Strength Aluminum Alloys, Materials and Manufacturing Processes, 2012, 27(6), 658–663.
[65] M. Thomas, F. Vollert, J. Weidemann, J. Gibmeier, A. Kromm, T. Kannengießer, Surface- and volume-based investigation on influences of different Varestraint testing parameters and chemical compositions on solidification cracking in LTT filler metals, Welding in the World, 2020, 64, 913-923.
[66] S. Singh, J. Andersson, Hot cracking in cast alloy 718, Science and Technology of Welding and Joining, 2018, 23(7), 568–574.
[67] W. Lin, J.C. Lippold, W.A. Baeslack III, An evaluation of heat-affected zone liquation cracking susceptibility, Part I: Development of a method for quantification, Welding Journal-New York, 1993, vol. 72, 135–153.
[68] J.C. Lippold, J.W. Sowards, G.M. Murray, B.T. Alexandrov, A.J. Ramirez, Weld solidification cracking in solid-solution strengthened Ni-base filler metals, in Hot Cracking Phenomena in Welds II, 2008, 147–170.
[69] J.E. Ramirez, Susceptibility of IN740 to HAZ Liquation Cracking and Ductility-Dip Cracking, Welding Journal, 2012, 91(4), 122–131.
[70] E.F. Nippes, W.F. Savage, An investigation of the hot ductility of high-temperature alloys, Welding Journal, 1955, 34(4), 183s–196s.
[71] S.T. Mandziej, Testing for Susceptibility to Hot Cracking on Gleeble™ Physical Simulator, Hot cracking phenomena in welds, 2005, 347–376.
[72] J. Andersson, J. Jacobsson, C. Lundin, A Historical Perspective on Varestraint Testing and the Importance of Testing Parameters, Cracking Phenomena in Welds IV. Springer International Publishing, 2016, 3-23.
[73] Standard Test Methods for Determining Average Grain Size, ASTM International, no. E112-96, 2004.
[74] J.K. Hong, J.H. Park, N.K. Park, I.S. Eom, M.B. Kim, C.Y. Kang, Microstructures and mechanical properties of Inconel 718 welds by CO_2 laser welding, Journal of Materials Processing Technology, 2008, 201(1–3), 515–520.
[75] S. Benhadad, N.L. Richards, and M.C. Chaturvedi, The influence of minor elements on the weldability of an INCONEL 718-type superalloy, Metallurgical and Materials Transactions A, 2002, 33(7), 2005–2017.
[76] T. J. Kelly, Elemental effects on cast 718 weldability, Welding Journal, 1989, 68(2), 44s–51s.
[77] F. Hanning, A.K. Khan, J. Andersson, O. Ojo, Advanced microstructural characterisation of cast ATI 718Plus®—effect of homogenisation heat treatments on secondary phases and repair welding behaviour, Welding in the World, 2020, 64(3), 523–533.
[78] B. Radhakrishnan, R.G. Thompson, A model for the formation and solidification of grain boundary liquid in the heat-affected zone (HAZ) of welds, Metallurgical and Materials Transactions A, 1992, 23(6), 1783–1799.
[79] D.A. Porter, K.E. Easterling, M.Y. Sherif, Phase Transformations in Metals and Alloys, (Revised reprint) 2009, CRC Press.

[80] M.S.A. Karunaratne, R.C. Reed, Interdiffusion of niobium and molybdenum in nickel between 900-1300 C, Defect and Diffusion forum, Trans Tech Publications Ltd, 2005, vol. 237, 420-425.